A land-to-ocean perspective on the magnitude, source and implication of DIC flux from major Arctic rivers to the Arctic Ocean

Suzanne E. Tank,[1,2] Peter A. Raymond,[3] Robert G. Striegl,[4] James W. McClelland,[5] Robert M. Holmes,[6] Greg J. Fiske,[6] and Bruce J. Peterson[1]

Received 23 August 2011; revised 7 May 2012; accepted 20 October 2012; published 14 December 2012.

[1] A series of seasonally distributed measurements from the six largest Arctic rivers (the Ob', Yenisey, Lena, Kolyma, Yukon and Mackenzie) was used to examine the magnitude and significance of Arctic riverine DIC flux to larger scale C dynamics within the Arctic system. DIC concentration showed considerable, and synchronous, seasonal variation across these six large Arctic rivers, which have an estimated combined annual DIC flux of 30 Tg C yr^{-1}. By examining the relationship between DIC flux and landscape variables known to regulate riverine DIC, we extrapolate to a DIC flux of 57 $\pm$ 9.9 Tg C yr^{-1} for the full pan-arctic basin, and show that DIC export increases with runoff, the extent of carbonate rocks and glacial coverage, but decreases with permafrost extent. This pan-arctic riverine DIC estimate represents 13–15% of the total global DIC flux. The annual flux of selected ions (HCO_3^-, Na^+, Ca^{2+}, Mg^{2+}, Sr^{2+}, and Cl^-) from the six largest Arctic rivers confirms that chemical weathering is dominated by inputs from carbonate rocks in the North American watersheds, but points to a more important role for silicate rocks in Siberian watersheds. In the coastal ocean, river water-induced decreases in aragonite saturation (i.e., an ocean acidification effect) appears to be much more pronounced in Siberia than in the North American Arctic, and stronger in the winter and spring than in the late summer. Accounting for seasonal variation in the flux of DIC and other major ions gives a much clearer understanding of the importance of riverine DIC within the broader pan-arctic C cycle.

Citation: Tank, S. E., P. A. Raymond, R. G. Striegl, J. W. McClelland, R. M. Holmes, G. J. Fiske, and B. J. Peterson (2012), A land-to-ocean perspective on the magnitude, source and implication of DIC flux from major Arctic rivers to the Arctic Ocean, *Global Biogeochem. Cycles*, *26*, GB4018, doi:10.1029/2011GB004192.

1. Introduction

[2] The Arctic Ocean watershed encompasses over 15% of the global terrestrial landmass, and is changing rapidly. The hydrologic cycle is intensifying throughout the Arctic region [*Rawlins et al.*, 2010], leading to a several-decades trend in increasing discharge from Eurasian rivers [*Peterson et al.*, 2002; *McClelland et al.*, 2006], and increasing discharge from North American rivers beginning in 1989 [*Déry et al.*, 2009]. In addition, active layers are deepening in both Siberia and the North American Arctic [*Oelke et al.*, 2004], while treelines are advancing [*Harsch et al.*, 2009]. These changes, among others, can be expected to lead to an altered biogeochemical signature in rivers throughout the pan-arctic [e.g., *Frey and McClelland*, 2009], and changes in the flux of numerous biogeochemical constituents, including dissolved organic C (DOC), dissolved inorganic C (DIC), and dissolved inorganic and organic N have already been observed [*Striegl et al.*, 2005; *McClelland et al.*, 2007; *Walvoord and Striegl*, 2007]. At the same time, the Arctic Ocean is small relative to its large catchment, and therefore particularly influenced by inputs from land [*McClelland et al.*, 2012], and susceptible to the ongoing change occurring throughout its watershed.

[3] Despite the clear importance of rivers to the larger Arctic system, until recently there was no methodologically consistent set of measurements of the biogeochemical composition of the world's major circumpolar rivers [*McClelland et al.*, 2008]. While the composition of large high latitude North American rivers has been relatively well documented [*Dornblaser and Striegl*, 2007; *Striegl et al.*, 2007; *Emmerton et al.*, 2008], measurements from Eurasian rivers have been sporadic, and in some cases unreliable [e.g.,

[1]Marine Biological Laboratory, Woods Hole, Massachusetts, USA.
[2]Now at Department of Geography, York University, Toronto, Ontario, Canada.
[3]Yale School of Forestry and Environmental Studies, Yale University, Connecticut, USA.
[4]USGS, Boulder, Colorado, USA.
[5]Marine Science Institute, University of Texas at Austin, Port Aransas, Texas, USA.
[6]Woods Hole Research Center, Falmouth, Massachusetts, USA.

Corresponding author: S. E. Tank, Department of Geography, York University, Toronto, ON M3J 1P3, Canada. (tanks@yorku.ca)

0886-6236/12/2011GB004192

Holmes et al., 2000; *Holmes et al.*, 2001]. Apart from the Yukon River, published constituent measurements are also overwhelmingly from the summer, outside of the critical freshet and under-ice periods [*McClelland et al.*, 2008]. This lack of full seasonal coverage significantly impedes our ability to understand the true flux of riverine constituents because concentrations change markedly across the annual hydrograph, and extrapolation from limited summertime measurements can cause significant under- or over-estimates of yearly fluxes [*Holmes et al.*, 2012]. To address these issues, the PARTNERS Project (Pan-Arctic River Transport of Nutrients, Organic Matter, and Suspended Sediments [*McClelland et al.*, 2008]) was initiated to measure the biogeochemistry of the world's six largest circumpolar rivers: the Ob', Yenisey, Lena, Kolyma, Yukon, and Mackenzie, with sample collection distributed across the annual hydrologic cycle. These six rivers provide more than half of the freshwater flux to the Arctic Ocean, and drain a total catchment area of 10.9×10^6 km^2 [*Holmes et al.*, 2012]. The Arctic Great Rivers Observatory (Arctic-GRO; 2009-current) followed on PARTNERS (2003–2006), and continues to measure the biogeochemistry of these rivers using identical protocols, sampling sites, and similarly obtaining measurements throughout the year, with a focus on the freshet and under-ice periods. To date, data from these projects has led to significantly improved annual and seasonal estimates of the riverine flux of DOC and inorganic and organic nutrients to the Arctic Ocean [*Raymond et al.*, 2007; *Holmes et al.*, 2012], in addition to improved flow-weighted mean estimates of riverine alkalinity concentration [*Cooper et al.*, 2008].

[4] Both on land and in the ocean, DIC (the sum of $CO_{2(aq)}$/H_2CO_3, HCO_3^- and CO_3^{2-}) is an important component of the overall C cycle. On land, a majority of the HCO_3^- and CO_3^{2-} flux from rivers is derived from chemical weathering, which, with organic carbon storage on land, represents one of the two major terrestrial sinks for atmospheric CO_2. During chemical weathering, $CO_{2(aq)}$ (i.e., in equilibrium with H_2CO_3) is transformed to bicarbonate (HCO_3^-) which can be transported to the ocean. Chemical weathering produces bicarbonate as a result of reaction with either silicate or carbonate rock. Silicate weathering (1) causes all bicarbonate to be produced from CO_2 fixation. In the absence of pyrite oxidation (see section 3.5) or other sources of acid (but see *Perrin et al.* [2008]), carbonate weathering (2) causes half of the bicarbonate to be derived from CO_2, and the other half directly from rock dissolution. These reactions are shown using olivine and calcite as examples:

$$Mg_2SiO_4 + 4CO_2 + 4H_2O \rightarrow 2Mg^{2+} + 4HCO_3^- + H_4SiO_4 \quad (1)$$

$$CaCO_3 + CO_2 + H_2O \rightarrow Ca^{2+} + 2HCO_3^- \quad (2)$$

Thus, the composition of the weathering material directly regulates the degree to which that DIC acts as a CO_2 sink. Additionally, although both silicate and carbonate weathering, and the resulting land-to-ocean DIC flux, are an integral component of the terrestrial C sink [e.g., *Raymond and Cole*, 2003], they sequester C on very different time scales. While the weathering of silicates can sequester CO_2 over million-year time scales, carbonate weathering sequesters CO_2 on the scale of thousands to hundreds of thousands of years, as a result of CO_2 release during the biological sequestration of $CaCO_3$ from Ca^{2+} and HCO_3^- in the oceans [*Berner et al.*, 1983; *Sundquist*, 1991]. Two previous studies have presented estimates of silicate and carbonate weathering from Arctic watersheds, both using ratios of weathering constituents (Ca^{2+}, Na^+, Mg^{2+} and Sr^{2+}) derived from point measurements: *Millot et al.* [2003], who undertook a detailed, subcatchment-specific analysis of weathering in the Mackenzie basin, and *Gaillardet et al.* [1999], who include all six PARTNERS rivers in an assessment of weathering in the world's 60 largest watersheds. Despite their clear contribution, however, neither study assessed how the known seasonal variation in constituent concentrations might affect estimates of weathering source.

[5] While river water is the main source of bicarbonate to the global ocean, the burial of $CaCO_3$ in sediments, after calcification by marine organisms, is its main sink [*Mackenzie and Garrels*, 1966]. There are increasing concerns about the saturation state of $CaCO_3$ in the world's oceans, as increasing atmospheric CO_2 dissolves in the ocean and decreases oceanic pH and thus the concentration of CO_3^{2-} [*Feely et al.*, 2004]. This in turn decreases the saturation state of calcite (Ω_{calc}), and in particular aragonite (Ω_{arag}), the more soluble mineral phase of $CaCO_3$. The saturation state is determined as:

$$\Omega = \frac{[Ca^{2+}][CO_3^{2-}]}{K'_{sp}}, \quad (3)$$

where K'_{sp} is the solubility product for either calcite or aragonite. When Ω falls below 1, shell and skeleton dissolution of calcifyers can occur, with consequent major biological and ecological implications [*Doney et al.*, 2009]. Numerous calcifying organisms exist in the Arctic Ocean, and because of its cold temperatures, this region is particularly susceptible to ocean acidification [*Steinacher et al.*, 2009]. Several sites with surface $\Omega_{arag} < 1$ have been documented within the Western Arctic Ocean and Bering Sea, particularly in regions where river water or sea ice melt appear to have diluted seawater $CaCO_3$ [e.g., *Bates*, 2006; *Bates et al.*, 2009; *Mathis et al.*, 2011; *Yamamoto-Kawai et al.*, 2011].

[6] In this paper, we use the seasonally representative PARTNERS and Arctic-GRO data sets to develop a cohesive, land-to-ocean perspective on the importance and implication of riverine DIC within the pan-arctic region. Specifically, we: (a) calculate a best estimate for DIC flux from each of the six PARTNERS rivers, using the USGS LoadEstimator modeling approach [*Runkel et al.*, 2004]; (b) use these flux estimates in concert with data on known regulators of riverine DIC to model the land-to-ocean export of DIC throughout the full pan-arctic catchment; (c) develop yearly flux estimates for major weathering constituents, and use these data to assess the weathering source of DIC within these catchments; and (d) assemble climatologies for DIC, alkalinity, and Ca^{2+}, and use these, with temperature, to assess the seasonal and geographic variation in the effect of rivers on Ω_{arag} in the Arctic Ocean nearshore. This work both refines previous estimates, and provides new information that

will shed additional light on the importance of riverine DIC within the larger pan-arctic C cycle.

2. Methods

2.1. Sample Collection and Analysis

[7] Constituent concentration data were obtained from the PARTNERS (2003–2006) and Arctic-GRO (data from 2009) project data sets, available online at the Cooperative Arctic Data and Information Service (CADIS) and Arctic Great Rivers Observatory websites (http://aoincadis.ucar.edu; http://arcticgreatrivers.org). Sampling sites were identical for both projects and located as close to river mouths, but above tidal influence, as possible, at Salekhard (Ob'), Dudinka (Yenisey), Zhigansk (Lena), Cherskiy (Kolyma), Pilot Station (Yukon), and Tsiigehtchic (Mackenzie). The sample collection scheme was designed to ensure coverage of base flow (under ice), spring melt, and late summer conditions, and emphasized the same sample collection methodology on each of the six rivers [see *McClelland et al.*, 2008].

[8] The PARTNERS and Arctic-GRO sampling protocol has been described in detail elsewhere [*Raymond et al.*, 2007; *Holmes et al.*, 2012]. The open-water collection scheme was modeled on the USGS equal discharge increment sampling protocol. Five depth-integrated samples were collected across the river channel on each sampling date using a USGS D-96 depth-integrating sampler fitted with a Teflon nozzle and Teflon collecting bag. The samples were combined in a 14-L Teflon churn to form a composite sample intended to account for within-river vertical and horizontal heterogeneity. Under-ice samples were collected near the water surface, from a single, mid-channel hole in the ice. Direct measures of surface water temperature were taken at the mid-channel sampling location. During the open water season, pH was measured on a D-96 depth-integrated sample from the mid-channel sampling location. Under-ice pH was measured on near-surface water at the mid-channel sampling hole.

[9] Samples for total alkalinity, major ions, and Sr were immediately filtered through an Aquaprep-600 capsule filter (Pall Corporation, 0.45 μm pore size) into high density polyethylene (HDPE) bottles. Major cation (here, Ca^{2+}, Na^{+} and Mg^{2+}) samples were immediately preserved with HCl to pH 2–3. Samples for Sr were filtered directly into Trace-Clean (VWR) HDPE bottles, which were shipped to sample sites enclosed in a sealed bag, and returned to the bag after sample collection. Collection and analysis techniques for DOC, which was used to calculate the organic anion contribution to alkalinity, are described elsewhere [*Raymond et al.*, 2007]. All samples were shipped refrigerated to Woods Hole, MA, USA, and distributed for analyses.

[10] Total alkalinity was analyzed at the Ecosystems Center in Woods Hole, by titrating samples with 0.16 N H_2SO_4 using a Hach digital titrator and WTW pH 315i meter equipped with a SenTix 81 probe, calibrated at pH 4.01 and 7.00 (WTW Inc., Gold River CA). Alkalinity was calculated using the Gran method with the online USGS calculator (http://or.water.usgs.gov/alk/). Major cations were analyzed at the Woods Hole Research Center using a Dionex Ion Chromatography system (GP50, AS50 and ED50; Dionex Corp.) fit with an IonPac CS12A analytical column, CG12A guard column, and CSRS Ultra II suppressor, using methanesulfonic acid as the eluent. Anions (Cl^{-} and SO_4^{2-}) were similarly analyzed using an IonPac AS14 analytical column, AG14 guard column, ASRS Ultra II suppressor, and sodium carbonate/sodium bicarbonate as the eluent. Sr was analyzed at the University of Southern Mississippi using inductively coupled plasma-mass spectrometry (ICPMS), as described by *Shiller* [2003].

[11] For each sample, we calculated carbonate alkalinity by estimating the alkalinity contribution of organic anions and subtracting this estimate from the total alkalinity measurement. The contribution of organic anions was estimated by calculating the charge of dissociated organic anions at the initial and Gran F3 endpoint pH ($\sim$pH 4.6) of each alkalinity titration using DOC concentration [*Oliver et al.*, 1983], and was always small (see section 3.1). DIC was then calculated from carbonate alkalinity and pH using the dissociation constants of *Millero* [2010] for carbonic acid and *Millero* [1979] for water. We did not correct our dissociation constants for the ionic strength of these waters because their low ionic concentration, from 0.8 to 5.4 meq L^{-1} across all rivers and sample dates, is below the range of salinities for which correction factors have been measured (equivalent to a salinity range of 0.04 to 0.27) [*Millero*, 2010].

2.2. Modeling Constituent Flux From PARTNERS Rivers to the Arctic Ocean

[12] We modeled the load of DIC, alkalinity, major ions, and Sr in the six largest Arctic rivers using the LoadRunner software package [*Booth et al.*, 2007] to automate runs of the USGS LoadEstimator program (LOADEST [*Runkel et al.*, 2004]). LOADEST uses a time series of paired streamflow and constituent concentration data to construct a calibration regression, which is then applied to a daily discharge record to obtain daily constituent loads (mass day^{-1}). The parameters for each of the calibration equations are provided on the CADIS website. We restricted our analyses to exclude all models containing long-term time functions because our short data series did not lend itself to detecting these trends. The Adjusted Maximum Likelihood Estimator (AMLE) was used to fit the calibration equation, and Akaike's Information Criterion was used to choose the model of best fit, with a further assessment to ensure that the slope of the measured: modeled data fit was never significantly different than 1 (α = 0.05).

[13] All discharge measurements were from gauging stations. On the Ob', Yukon, and Mackenzie Rivers, constituent sampling sites were identical to the gauging station location. On the Yenisey, Lena, and Kolyma Rivers, proximate gauging stations were used, at Kyusyur, Igarka, and Kolymskoye, respectively. We corrected for temporal offsets between sampling and gauging locations using the lag-time estimates described in *Holmes et al.* [2012].

[14] We obtained daily discharge for a 10 year period between 2000 and 2009 from the ArcticRIMS Project (http://rims.unh.edu) for the Ob', Yenisey, and Lena Rivers, the Water Survey of Canada for the Mackenzie River, and the USGS for the Yukon River. Discharge data for the Kolyma River was provided by Alexander Shiklomanov (Water Systems Analysis Group, University of New Hampshire). For DIC and carbonate alkalinity, LOADEST calibration equations were determined using PARTNERS and Arctic-GRO constituent data from 2003 to 2009. For major ions and Sr, PARTNERS data from 2003 to 2006 were used. In both

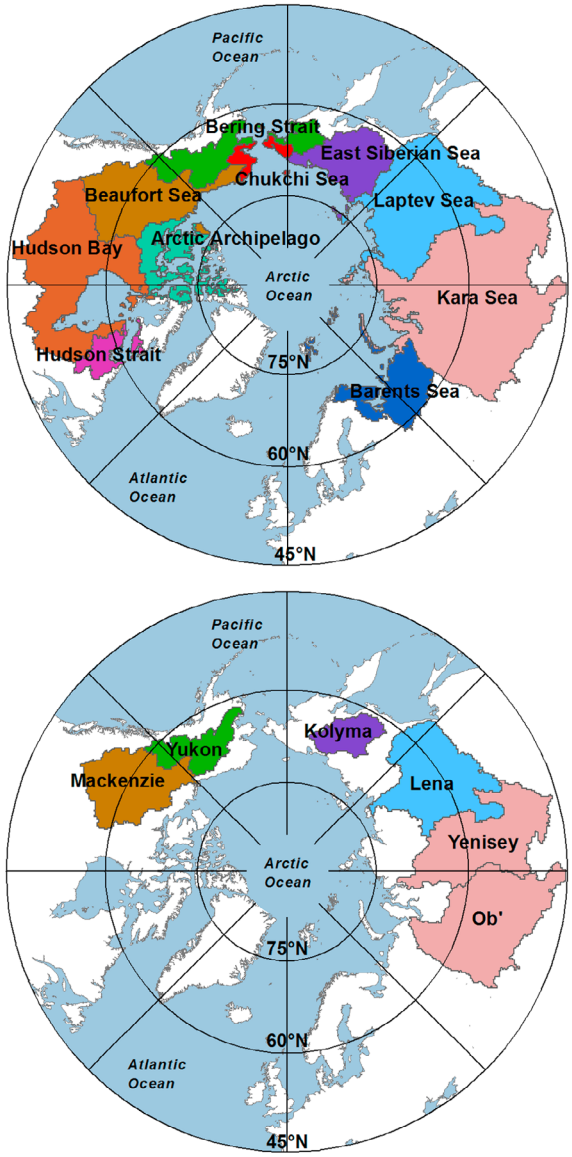

Figure 1. (top) The 10 major sea basins of the Arctic Ocean, from *Lammers et al.* [2001]. Note that the Bering Strait and Chukchi sea basins span the North American and Eurasian landmasses. (bottom) The six PARTNERS watersheds. The color of each watershed is identical to the sea basin within which it lies.

cases the LOADEST calibration equation was used to extrapolate fluxes to the 10 year discharge data period. Any data gaps in the discharge record were filled by interpolation; there were no gaps during the peak flow period on any river. For the Yukon River, discharge data are from 2001 to 2009, and 9 years of constituent flux are presented.

2.3. Extrapolating DIC Flux to the Full Pan-Arctic Basin

[15] We estimated DIC flux to the full Arctic Ocean basin using the runoff data for each of the ten Arctic Ocean sea basins provided in *Lammers et al.* [2001] (Figure 1), in addition to data on lithology, permafrost extent, and glacial coverage. For each of the six PARTNERS watersheds and ten Arctic Ocean sea basins, we calculated the percent coverage of each of the lithologic classes from the *Dürr et al.* [2005] digital lithologic map, and the percent coverage of each of the permafrost classes from *Brown et al.* [1998]. Because glacial weathering can be a significant source of inorganic C [*Anderson et al.*, 2000; *Striegl et al.*, 2007], we also obtained data on the percent glacial coverage within each watershed and sea basin from *Kaser et al.* [2010], the *World Glacier Monitoring Service* [1989], and the World Glacier Inventory online database housed at the National Snow and Ice Data Center (http://nsidc.org/data/g01130.html).

[16] We predicted DIC flux (Tg C yr^{-1}) within each of the major sea basins by using multiple linear regression to correlate DIC yield to runoff, lithology, permafrost extent and glacial coverage within the PARTNERS watersheds, extrapolating the yield relationship to each sea basin area not contained within a PARTNERS watershed, and converting DIC yields to fluxes using the catchment area of each sea basin, as determined from the ArcticRIMS drainage system information. Only significant predictor variables ($\alpha = 0.05$) were included in our prediction equation, and the best model was selected using Akaike's Information Criterion. Because the extent of glaciers in the Arctic Archipelago is very poorly constrained [*Cogley*, 2010] and the effect of glacial weathering is likely different in the High Arctic than in more southerly Arctic locations (see further discussion in section 3.3), DIC flux from this sea basin was calculated without this term.

[17] One potential source of error in using the PARTNERS watersheds to extrapolate pan-arctic DIC fluxes is a lack of sample coverage across the western Eurasian and eastern North American Arctic (Figure 1). To assess the validity of our model for areas outside the six PARTNERS watersheds, we calculated a weighted mean of the DIC yield from rivers within the relatively limestone-rich Hudson Bay sea basin using the regional discharge and catchment area data reported in *Déry et al.* [2005] and concentration data from various sources [*Environment Canada*, 1978; *Meybeck and Ragu*, 1995], and compared this to our model-predicted DIC yield from this region. We further compared modeled and literature-reported DIC yields for the Indigirka watershed, which unlike the Hudson Bay region is silicate-rich, almost entirely underlain by permafrost, and contains a relatively high proportion of glaciers [*Kaser et al.*, 2010].

2.4. Assessing the Source of DIC in Major Arctic Rivers

[18] We assessed the weathering-derived source of non-CO_2 DIC (i.e., $HCO_3^- + CO_3^{2-}$) to each of the six PARTNERS rivers using a modification of the inverse modeling approach presented by *Gaillardet et al.* [1999], which takes advantage of the fact that weathering of different rock types (e.g., carbonates versus silicates) results in the release of ions in characteristic ratios. The *Gaillardet et al.* [1999] mixing model takes the form (for X = Ca^{2+}, Mg^{2+}, $[HCO_3^- + CO_3^{2-}]$, Sr^{2+} and Cl^-):

$$\left(\frac{X}{Na}\right)_{river} = \sum_i \left(\frac{X}{Na}\right)_i \alpha_i \,(Na) \qquad (4)$$

where i refers to the various end-member types and α_i are the mixing proportions of Na^+, which sum to 1.

[19] For each of the six rivers, annual fluxes of Na^+, Ca^{2+}, Mg^{2+}, $[HCO_3^- + CO_3^{2-}]$, Sr^{2+} and Cl^- were calculated as

Table 1. Mean of Annual Discharge and LOADEST-Modeled Constituent Flux From Major Arctic Rivers[a]

	Ob'	Yenisey	Lena	Kolyma	Yukon	Mackenzie	Total
Discharge ($km^3\ y^{-1}$)	418 (71)	636 (39)	594 (85)	106 (20)	208 (19)	305 (26)	2267 (150)
DIC (Tg C y^{-1})	5.90 (0.25)	6.96 (0.18)	5.82 (0.73)	0.81 (0.10)	4.45 (0.23)	6.29 (0.43)	30.23 (1.19)
HCO_3^-+CO_3^{2-} (Tg C y^{-1})	4.94 (0.32)	6.57 (0.17)	5.47 (0.69)	0.58 (0.09)	4.04 (0.24)	5.83 (0.43)	27.42 (1.20)
Ca (Tg y^{-1})	6.62 (0.60)	11.40 (0.38)	9.18 (1.24)	1.19 (0.20)	6.43 (0.47)	10.74 (0.94)	45.56 (2.34)
Na (Tg y^{-1})	2.65 (0.26)	4.09 (0.17)	5.35 (0.37)	0.16 (0.02)	0.55 (0.03)	2.35 (0.09)	15.15 (0.60)
Mg (Tg y^{-1})	1.75 (0.13)	2.44 (0.11)	2.68 (0.39)	0.25 (0.04)	1.54 (0.09)	2.92 (0.22)	11.58 (0.65)
Cl (Tg y^{-1})	2.29 (0.20)	6.20 (0.26)	10.39 (0.58)	0.03 (0.01)	0.19 (0.01)	3.07 (0.05)	22.17 (0.77)
Sr (Gg y^{-1})	42 (4)	84 (2)	67 (7)	6 (1)[b]	26 (2)	58 (3)	283 (12)
SO_4 (Tg S y^{-1})	1.06 (0.11)	1.96 (0.09)	2.38 (0.25)	0.36 (0.05)	2.14 (0.13)	4.80 (0.28)	12.70 (0.59)

[a]Means are for 2000–2009, except for the Yukon River, which is for 2001–2009. Brackets indicate standard deviation of the 10-year time series mean.
[b]Flux calculated from daily discharge using the relationship between concentration and discharge; the number of data points was insufficient for LOADEST.

described in section 2.2. Annual fluxes were corrected for rainwater inputs, and end-members for carbonate, felsic silicate, basaltic, and evaporite rocks were obtained from previously published data as described in the auxiliary material.[1] Because weathering ions can be temporarily, and selectively, stored in vegetation after they are weathered, our use of annual flux ratios acts to integrate fluxes over periods of active uptake (e.g., summer) and release via plant decomposition (e.g., spring and fall) [*Zakharova et al.*, 2007].

[20] Models were run using the Bayesian mixing model platform MixSIR [*Moore and Semmens*, 2008], which allows specification of end-members, end-member standard deviations, and multiple mixture (here, river water) data points, and iteratively generates a distribution to describe the range of possible source contributions to the mixture. The model output was converted to source proportions of (HCO_3^- + CO_3^{2-}) using the various end-member HCO_3^-/Na^+ ratios. The model was run multiple times for each river. For all rivers, we ran the model using a base set of end-members with the river water mixture corrected using minimum, mean, and maximum rainwater correction, to allow for a sensitivity analysis of the effect of the rainwater correction on our estimates. For the Mackenzie, Yukon, Ob' and Kolyma Rivers, this base set of end-members included carbonate, felsic silicate, and evaporite rocks. For the Yenisey and Lena Rivers we added a catchment-specific saline groundwater end-member to our base set of end-members. Finally, to assess the possible contribution of basalts to HCO_3, we ran the model substituting the basaltic for the felsic end-member for rivers that have substantial basaltic rock in their catchment (Yenisey, Lena, Ob' and Kolyma). Values for each of the end-members are provided in Table S1 in the auxiliary material. For each model output, the modeled Σ_i ($[HCO_3^- + CO_3^{2-}]/Na^+)_i$ was checked against the true, yearly $[HCO_3^- + CO_3^{2-}]$:Na^+ ratio.

2.5. Seasonal Impacts of Riverine DIC on Aragonite Saturation in the Arctic Ocean

[21] We explored the seasonal variation of the effect of river water on coastal aragonite saturation in two ways. First, we calculated monthly climatologies for alkalinity, Ca^{2+} and DIC concentration on each of the PARTNERS rivers, by averaging LOADEST concentration outputs (available on the CADIS website) within monthly bins. Second, we used the LOADEST outputs to estimate Ω_{arag} over an estuarine-to-ocean salinity gradient during the spring freshet and late-summer periods. For the freshwater end-member, we calculated the flow-weighted mean concentration of Ca^{2+}, alkalinity, and DIC in June, when peak discharge levels cause the maximum dilution of inorganic constituents, and August–September, the end of summer. We did this for three distinct river groupings that display similar within-river concentrations of these constituents (see sections 3.1 and 3.2): the North American rivers (Mackenzie and Yukon), central Siberian rivers (Ob' Yenisey and Lena), and the Kolyma River. The oceanic end-member for Ca^{2+} was calculated using the common relationship with salinity [*Riley and Tongudai*, 1967]. Oceanic alkalinity and DIC were taken as the spring-summer value at the bottom of the polar mixed layer from *Bates et al.* [2009] (alkalinity = 2240 μeq L^{-1}, DIC = 2100 μmol L^{-1}). Alkalinity, DIC, and Ca^{2+} were varied linearly with salinity, and CO_3^{2-} was calculated from alkalinity and DIC using the CO2SYS program [*Lewis and Wallace*, 1998], assuming T = 0°C (see section 3.6 for a discussion of the effect of our temperature assumption). We further calculated K_A, the solubility product for aragonite [*Mucci*, 1983] across the salinity gradient, and determined Ω_{arag} as in equation (3).

3. Results and Discussion

3.1. DIC Concentration and Flux From the Six Largest Arctic Rivers

[22] The total LOADEST-modeled oceanic flux of DIC from the six largest Arctic rivers was 30 Tg C y^{-1} (Table 1). Yearly flow-weighted DIC concentrations were highest in North American rivers (21.5 and 20.6 mg L^{-1} for the Yukon and Mackenzie, respectively), moderate for Central Siberian rivers (14.1, 10.9, and 9.8 mg C L^{-1} for the Ob', Yenisey, and Lena), and low in the Kolyma River (7.7 mg L^{-1}). These marked differences in concentration caused yearly DIC flux from the relatively low discharge North American rivers to be similar to or greater than DIC flux from Central Siberian rivers, which have considerably higher discharge (Table 1). Across all rivers, 28% of the total DIC flux occurred during the spring freshet period (May–June), and a further 30% occurred under ice (Nov–April).

[23] The estimated contribution of organic acids to individual measurements of total alkalinity was always small, ranging from 0.3% under ice, when DIC concentrations are

[1]Auxiliary materials are available in the HTML. doi:10.1029/2011GB004192.

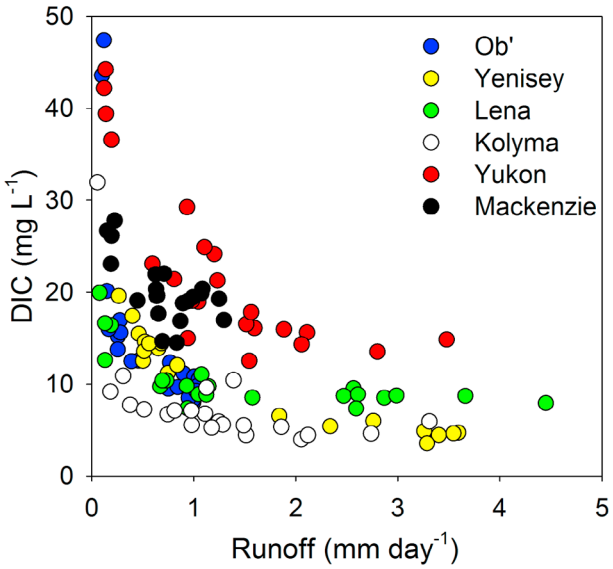

Figure 2. DIC concentrations in individual water samples from major Arctic rivers, calculated from carbonate (i.e., organic-ion corrected) alkalinity, temperature, and pH. DIC is plotted against daily discharge normalized to the watershed area (runoff).

high but DOC concentrations are low, to 6–10% during the peak of the freshet, when the opposite pattern occurs. Correction for organic acids decreased the estimate of total LOADEST-modeled DIC flux from the six PARTNERS rivers by ~4% (Table S2 in the auxiliary material). Concentrations of DIC calculated from pH and carbonate (i.e., organic acid corrected) alkalinity compare well to direct DIC measurements, which are available for a select number of samples collected on the Yukon River (analyses described in *Schuster* [2003]), and during the Arctic-GRO project (analyses described in the online data set at www.arcticgreatrivers.org). Calculated DIC concentrations tend to be skewed low at the highest (under ice) concentrations. Otherwise, the calculated: measured regression line is not significantly different than 1 (t_{28} = 0.477, p = 0.637, Figure S1 in the auxiliary material). Riverine DIC concentration shows a clear dilution at high flow, which leads to significant within-river variation in DIC concentration (Figure 2), ranging from 1.9-fold on the Mackenzie River to 8.0-fold on the Kolyma. Between rivers, measured DIC was highest in North American rivers, and lowest in the Kolyma River (Figure 2).

[24] LOADEST-modeled daily DIC fluxes were well correlated with directly calculated daily fluxes of DIC, with an r^2 for the measured: modeled relationship from individual rivers ranging from 0.83 to 0.99. The slopes of these relationships ranged from 0.84 to 0.99, and were never significantly different than 1 ($\alpha = 0.05$). The LOADEST-calculated 95% confidence interval for the mean annual DIC flux was ±1.7 Tg C yr^{-1}, and ranged from 3.6 to 10.7% of total flux across rivers. Detailed model outputs and model calibrations are available on the CADIS website; the LOADEST model output for each river is presented in Figure S2 in the auxiliary material.

[25] The percentage of LOADEST-modeled yearly DIC flux that was bicarbonate or carbonate (i.e., not present as CO_2) ranged from 72% in the Kolyma River to 91–94% in the Yenisey, Lena, Yukon, and Mackenzie (Table 1). Yearly fluxes of bicarbonate plus carbonate ($HCO_3^- + CO_3^{2-}$) were within 5% of the LOADEST-modeled carbonate alkalinity flux on all rivers (i.e., alkalinity corrected for organic anions; data not shown), in agreement with measured riverine pH (95% of measurements <8.2), which indicates very low within-river CO_3^{2-}. On all rivers except the Ob', these LOADEST-modeled carbonate alkalinity fluxes lie within 6% of the flow-weighted total alkalinity concentrations calculated by *Cooper et al.* [2008], who also used PARTNERS project data. For the Ob' River, our estimates are 17% less than those presented by *Cooper et al.* [2008].

[26] Using DOC flux estimates from *Holmes et al.* [2012], the ratio of DIC: DOC in the six largest Arctic rivers is 1.7. This is similar to the global DIC:DOC flux ratio, which is estimated at slightly below 2 (~1.9, using the estimated 0.23 Pg DOC flux yr^{-1} from *Schlünz and Schneider* [2000] and the estimated 0.44 Pg DIC flux yr^{-1} from *Meybeck* [1987]). However, the yearly DIC: DOC flux ratios show substantial variation across the Arctic Ocean basin: while DIC fluxes from the North American rivers are disproportionately high, the vast majority of DOC flux comes from Russia [*Raymond et al.*, 2007; *Holmes et al.*, 2012]. As a result, DIC:DOC is notably high in the North American rivers (3.8; combined river fluxes), but only 1.5 in the Ob' and Yenisey and 1.0 in the Lena and Kolyma. The implications of this spatial variation in DIC flux, and DIC: DOC flux ratios, are further discussed in section 3.6 below.

3.2. DIC Yields and Extrapolated Flux From the Full Pan-Arctic Basin

[27] Similar to the results for DIC concentration, the relationship between annual water yield (runoff; cm yr^{-1}) and annual DIC yield (g C m^{-2} yr^{-1}) differed significantly between the PARTNERS catchments and across the pan-arctic region (Figure 3). DIC yields were highest in western North American watersheds, intermediate in Central Siberian watersheds, and lowest in the Kolyma watershed (Figure 3).

[28] DIC yield was positively related to runoff, the presence of carbonates, and glacial coverage, and negatively related to continuous permafrost extent (Table 2). The DIC prediction equation had an adjusted r^2 of 0.919, and a slope slightly less than 1 (0.920; 95% confidence interval = 0.85–0.99; Figure 4). The percent coverage of basaltic rocks (Vb from *Dürr et al.* [2005]) was not a significant predictor variable, despite a previous global assessment indicating rapid weathering rates for basaltic rocks relative to felsic silicates [*Dessert et al.*, 2003]. Similar to the results of *Moosdorf et al.* [2011] for North America, the results of our prediction equation may indicate that the weathering history, or age, of basaltic rocks can influence their contemporary contribution to weathering and bicarbonate flux. Within each watershed and sea basin, we calculated a carbonate index as the sum of the median proportion of carbonates in classes Sc (carbonate rocks; 0.8) and Sm (mixed sedimentary; 0.4) [*Dürr et al.*, 2005] multiplied by the percent coverage of that class. This index was a better predictor of DIC yield than class Sc alone, or a more complete proportional carbonate index that also contained rock classes with much lower

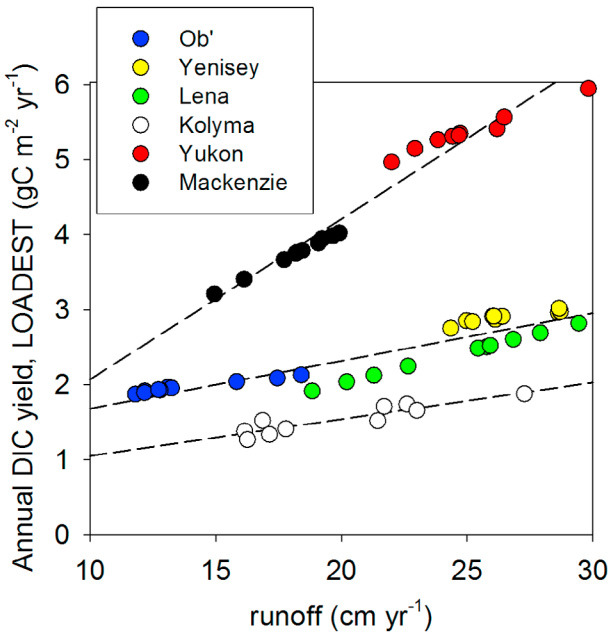

Figure 3. Yearly LOADEST-calculated DIC yields (DIC flux normalized to watershed area) plotted against yearly runoff (discharge normalized to watershed area) for each of the six PARTNERS rivers. Data points show individual years between 2000 and 2009.

carbonate contents (included Sc, Sm, Ss, Su and Lo). The important contribution of class Sm to bicarbonate flux has been shown in several other recent, regional assessments [*Hartmann et al.*, 2009; *Moosdorf et al.*, 2011]. Continuous permafrost was also a better predictor of DIC yield than the sum of all permafrost classes (continuous, discontinuous, sporadic and intermittent), or a permafrost index calculated as the percent coverage of each permafrost class multiplied by the median proportion of permafrost in that class.

[29] Using this prediction equation, we estimate DIC flux from the full Arctic Ocean watershed to be 57.2 Tg C yr^{-1}, and calculate a conservative 95% error bound of ±9.9 Tg C yr^{-1}, using the 95% confidence interval calculated by LOADEST for flux from the PARTNERS rivers, and the 95% prediction (rather than confidence) interval from the multiple linear regression model for sea basin areas outside of the PARTNERS catchments (R statistical software package) (Tables 2, 3, and S3). The few previous estimates of DIC flux from the full pan-arctic catchment are considered somewhat uncertain (see *McGuire et al.* [2010], who incorporate the Eurasian flux estimates of *Gordeev et al.* [1996] and *Vetrov and Romankevich* [2004]). Previous flux estimates were based on direct within-river extrapolations from concentration means, which typically include little to no representation of the winter and spring freshet periods, when DIC concentrations vary substantially from summertime values (Figure 2) [*McGuire et al.*, 2010]. Our extrapolated DIC flux is 5% higher than the 43.2 Tg C yr^{-1} estimated by *McGuire et al.* [2009] for the pan-arctic excluding Hudson Bay, Hudson Strait and the Bering Sea, but including the Yukon River (we estimate 45.3 Tg C yr^{-1} for the same region). Given that the *McGuire et al.* [2009] estimate does not include CO_2, which is also ~10% of the PARTNERS riverine flux, these estimates are remarkably close to one another using very different methodologies. For DIC, which dilutes at high flow (spring) and increases in concentration during periods of low flow (winter), extrapolating from summertime measurements may potentially provide a reasonable approximation of yearly fluxes, in contrast to the problems related to using summertime measurements to extrapolate fluxes for constituents that become more concentrated with increasing discharge (e.g., DOC) [*Raymond et al.*, 2007]. We do note, however, that there are some large discrepancies between our estimates and the *McGuire et al.* [2009] estimates at the sea basin scale, with the previous estimates being substantially higher than our Barents Sea estimate (54%), and substantially lower than our North American (33%) and Chukchi Sea (98%) estimates.

3.3. Model Validation

[30] To confirm the validity of our prediction model, we compared the modeled DIC yield for the Hudson Bay sea basin to a weighted mean yield derived from literature values. Published measures of DIC concentration range from below 4 mg L^{-1} for rivers on the northwest and eastern perimeter of the Bay, to greater than 20 mg L^{-1} for rivers flowing across the limestone rich terrain in the southwest

Table 2. Model Input Parameters Used to Predict DIC Yield From the 6 PARTNERS Watersheds[a]

	Carbonate Index	Basalts (%)	Continuous Permafrost (%)	Glacial Coverage (%)	Runoff (cm yr^{-1})	DIC Yield (g C m^{-2} yr^{-1})
			Watershed			
Ob'	1.1	0.8	1	0.040	14.0 (2.4)	1.97 (0.09)
Yenisey	10.6	12.1	31	0.002	26.5 (1.6)	2.90 (0.08)
Lena	20.6	2.4	77	0.003	24.4 (3.5)	2.40 (0.30)
Kolyma	2.1	11.9	99	0.000	20.0 (3.7)	1.54 (0.20)
Yukon	8.4	5.4	19	1.093	25.0 (2.3)	5.37 (0.27)
Mackenzie	16.4	1.1	13	0.035	18.2 (1.6)	3.74 (0.26)
			Model Parameters[b]			
Coefficient	0.056	NS	−0.013	2.254	0.045	
t_{54}	7.339	NS	−8.619	15.456	3.742	
p-value	<0.001	NS	<0.001	<0.001	<0.001	

[a]See text for calculation of carbonate index, basalts, permafrost, and glacial coverage. Runoff and DIC yield were calculated from known discharge, watershed area, and LOADEST-modeled DIC flux. NS = not significant; brackets indicate standard deviation of the 10-year time series mean. The model fit is illustrated in Figure 4.

[b]The coefficient for the model intercept is 1.550 (t_{54} = 7.305, p < 0.001).

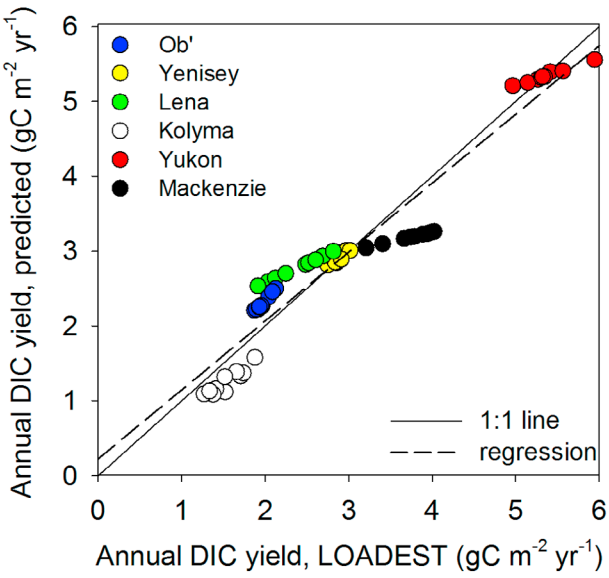

Figure 4. The relationship between LOADEST-calculated DIC yields, and yields predicted from runoff, lithology, permafrost, and glacial coverage, for the six PARTNERS catchments. The regression for the relationship is indicated by the dashed line; $y = 0.22 + 0.92x$. The prediction equation is given in Table 2 and regression statistics are given in the text.

(Figure 5) [*Environment Canada*, 1978; *Meybeck and Ragu*, 1995]. Of the 35 Hudson Bay rivers listed in *Déry et al.* [2005], we were able to locate concentration data for 14, which encompass ~80% of the total basin discharge. For rivers for which no concentration data were available, we grouped those outside of the limestone-rich lens into east- and west- shore assemblages and assigned these an average concentration using measurements from rivers within that same geographic area; we assigned rivers flowing over the limestone lens an average concentration calculated from concentrations measured on rivers in this region. Because the literature data that we obtained report bicarbonate concentrations rather than total DIC, and do not consistently report pH, we estimated total DIC concentration within each river by assuming that the proportion of DIC that is bicarbonate in soft water rivers (those outside the limestone-rich terrain) was similar to that on the Kolyma River, and the proportion of bicarbonate in rivers flowing over limestone-rich regions was similar to that found in the remaining, relatively bicarbonate-rich, PARTNERS rivers. The *Déry et al.* [2005] discharge and catchment area values were then used to calculate a weighted mean yield of 2.5 g C m^{-2} yr^{-1} (12 mg L^{-1} as a flow weighted concentration; Figure 5), which is within 20% of the modeled DIC yield of 3.0 g C m^{-2} yr^{-1} for this region (15 mg L^{-1} as a flow-weighted concentration), and well within the 95% prediction interval calculated for the Hudson Bay sea basin (Table 3 and Figure 5).

[31] We further compared modeled DIC yields for the Indigirka River to DIC yields derived from the published values of *Vetrov and Romankevich* [2004]. In contrast to the Hudson Bay region, the Indigirka is dominated by silicate rocks, entirely underlain by permafrost, and has glaciers within its catchment. For the literature derived estimate, we assumed a (HCO_3^- + CO_3^{2-}): CO_2 ratio identical to that on the neighboring, and similarly soft water, Kolyma, and calculated DIC yield based on discharge and catchment area data reported in *McGuire et al.* [2009]. Inputs for modeled DIC yield were from *McGuire et al.* [2009] (runoff), *Kaser et al.* [2010] (glacial coverage), the Arctic RIMS data set (rims.unh.edu; permafrost coverage) and *Dürr et al.* [2005] (lithology). The modeled DIC yield of 1.3 g C m^{-2} yr^{-1} was 11% less than the estimate of 1.4 g C m^{-2} yr^{-1} from literature values. Thus, it appears that our extrapolation model performs reasonably well across a broad range of lithologic, hydrologic, and cryospheric conditions, while our calculated 95% error bound provides a conservative bound on our extrapolated flux estimate.

3.4. Controls on Pan-Arctic DIC Flux

[32] The 57 Tg yr^{-1} pan-arctic DIC flux that we calculate represents 13–15% of global riverine DIC flux [*Meybeck*, 1987; *Aminotte Suchet and Probst*, 1995; *Gaillardet et al.*, 1999]. In contrast, the ten Arctic Ocean sea basins contribute ~12% of global river discharge (Table 1) [*Fekete et al.*,

Table 3. Modeled DIC Flux for the Ten Major Sea Basins of the Arctic Ocean[a]

Sea Basin	Area 10^6 km^2	Runoff (cm yr^{-1})	DIC Yield (g C m^{-2} yr^{-1})	DIC Flux (Tg yr^{-1})
Arctic Archipelago	1.13	16.4	2.6 (0.8)[b]	3.0 (1.0)[b]
Barents Sea	1.32	34.9	3.6 (0.8)	4.7 (1.1)
Beaufort Sea *(Mackenzie)*	2.14	20.0	3.5 (0.2)	7.6 (0.5)
Bering Sea *(Yukon)*	1.21	25.6	4.2 (0.5)	5.1 (0.6)
Chukchi Sea	0.28	51.1	3.5 (1.0)	1.0 (0.3)
East Siberian Sea *(Kolyma)*	1.33	18.1	1.3 (0.5)	1.7 (0.6)
Hudson Bay	3.30	19.2	3.0 (0.7)	9.8 (2.5)
Hudson Strait	0.45	50.8	3.4 (1.1)	1.5 (0.5)
Kara Sea *(Ob', Yenisey)*	6.63	18.6	2.2 (0.3)	14.7 (1.7)
Laptev Sea *(Lena)*	3.64	21.0	2.3 (0.3)	8.2 (1.2)
SUM	21.44			57.2 (9.9)

[a]DIC yield was obtained directly from the LOADEST output, or calculated using the model parameters given in Table 2 for sea basin regions outside of the PARTNERS watersheds. Flux was obtained using sea basin areas derived from the Arctic RIMS database. Brackets indicate ±95% error bound, based on the LOADEST-modeled confidence interval for the PARTNERS rivers, and the 95% prediction interval from the multiple linear regression model. PARTNERS rivers within each sea basin are indicted beside the seas basin name. Full calculation details are provided in Table S3 in the auxiliary material.
[b]Calculated without the glacial coverage term.

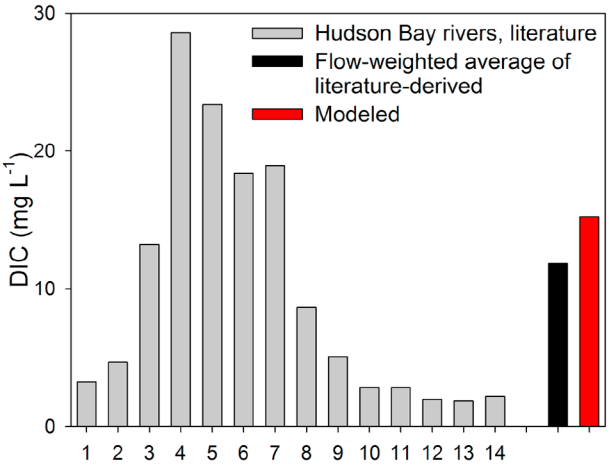

Figure 5. Literature-derived DIC concentrations for rivers in the Hudson Bay sea basin (gray), shown counterclockwise around the Bay from the northwest corner. Higher DIC concentrations in rivers 3–8 corresponds to a limestone-rich region along the Bay's southwest perimeter. A flow-weighted average concentration for the sea basin, calculated from the literature-derived concentrations as described in the text, is shown in black. The modeled sea basin estimate, based on runoff, permafrost, lithology, and glaciers is shown in red. River legend: 1: Chesterfield Inlet, 2: Seal, 3: Churchill, 4: Nelson, 5: Hayes, 6: Albany, 7: Moose, 8: Harricana, 9: Nottaway, 10: Broadback, 11: Rupert, 12: Eastmain, 13: La Grande, 14: Grande Baleine. Data are from *Environment Canada* [1978] and *Meybeck and Ragu* [1995].

2002], indicating that rivers flowing to the Arctic Ocean are slightly above the global DIC mean. While average runoff to the Arctic Ocean is somewhat lower than the global average [*Lammers et al.*, 2001; *Fekete et al.*, 2002], and silicate weathering rates may decrease with decreasing temperature (reviewed in *Louvat et al.* [2008]), the Arctic Ocean catchment is carbonate rich, with the ten Arctic Ocean sea basins containing 20% of the global extent of consolidated carbonates (calculated from *Dürr et al.* [2005]). Not surprisingly, given the rapid weathering rate for carbonate rock and its known importance to DIC flux [*Meybeck*, 1987], our model indicates that DIC yield is positively related to carbonate rock coverage across these Arctic catchments.

[33] Glacial extent was also a positive predictor of DIC yields in our model. Weathering by temperate glaciers (composed of ice at its melting point; in contrast to cold-based glaciers) is known to significantly increase DIC flux from glaciated catchments, because the production of glacial flour makes dispersed carbonate deposits readily accessible to chemical weathering [*Sharp et al.*, 1995; *Tranter et al.*, 1997; *Anderson et al.*, 2000]. Thus, glacial outlet water that comes into contact with subglacial sediments [e.g., *Sharp et al.*, 1995; *Tranter et al.*, 1997], and in particular water flowing over proglacial sediment deposits [*Anderson et al.*, 2000], can be considerably DIC-enriched. Carbonate denudation is so favored in glaciated catchments that the weathering signal and DIC concentration of export waters can mimic that found over carbonate terrains, even when the underlying bedrock is overwhelmingly silicate [*Anderson et al.*, 2000].

[34] Outside of the Arctic Archipelago and Eurasian Arctic Islands, Arctic glaciers are by far most prevalent in the Yukon River basin, where both DIC and particulate inorganic C (PIC) flux from glaciated catchments is considerable, and approximately 30% of PIC is weathered to bicarbonate during downstream transport [*Striegl et al.*, 2007]. However, we note that glaciers cover only 1% of the Yukon catchment, while the Yukon DIC yield is significantly higher than would be predicted based upon runoff and the apparent extent of carbonate rocks (Table 2). Thus, it seems probable that rock types not captured in our carbonate index also contribute significantly to DIC flux in the Yukon River basin, likely as a result of the trace minerals that can be contained in many non-carbonate rock types [*Hartmann et al.*, 2009; *Moosdorf et al.*, 2011]. In the Yukon River basin, class Cl (complex lithology) is a good candidate for this discrepancy because it covers nearly 25% of the Yukon basin and is composed of mixed rock associations [*Dürr et al.*, 2005]. A more nuanced, sub-basin specific assessment of DIC origin within the Yukon River watershed would significantly improve our understanding of weathering processes in this region [see also *Striegl et al.*, 2007].

[35] We did not include glaciers from the Canadian Arctic Archipelago or Eurasian Arctic Islands in our assessment. In part, this was because glacial coverage in the Canadian Archipelago is poorly documented [*Cogley*, 2010]. However, cold-based and polythermal (mixed cold and temperate ice) glaciers also exhibit fundamentally different glacial flow paths and thus opportunities for water-rock interaction than their temperate counterparts, indicating that the effect of glaciers on DIC flux in the High Arctic may differ from that at more southern Arctic locations such as the Yukon River Basin [*Hodson et al.*, 2000; *Wadham et al.*, 2010]. For example, while the flux of DIC from smaller, entirely cold-based glaciers may be low [*Hodgkins et al.*, 1997; *Hodson et al.*, 2000], solute flux from the polythermal Antarctic Ice Sheet exhibits DIC concentrations that are double oceanic values [*Wadham et al.*, 2010], despite theory predicting that large ice sheets should act as barriers to weathering [*Kump and Alley*, 1994]. While we do not draw conclusions about the current effect of High Arctic glaciers on DIC flux, we note that DIC export from recently uncovered High Arctic proglacial sediments can be as elevated as the proglacial export from more southerly Arctic locations [*Wadham et al.*, 2001]. Thus, the current High Arctic glacial retreat [*Gardner et al.*, 2011] could certainly cause a notable, future increase in DIC flux from this region.

[36] In contrast to runoff, carbonates, and glaciers, the extent of continuous permafrost was a significant negative predictor of DIC yield. Several studies have shown that the presence of permafrost causes a decrease in the export of major ions, because permafrost limits the interaction between rock and surface waters while also blocking mineral-rich groundwater from reaching surface flowpaths (reviewed in *Frey and McClelland* [2009]). In the Yukon and Ob' basins, sub-catchments underlain by permafrost have significantly lower concentrations of DIC and other weathering-derived ions compared to their non-permafrost associated counterparts [*Frey et al.*, 2007; *Walvoord and Striegl*, 2007]. The recent increase in active layer depth through much of the pan-arctic region [*Oelke et al.*, 2004], and contemporary increases in base flow and flow from deeper soil horizons documented

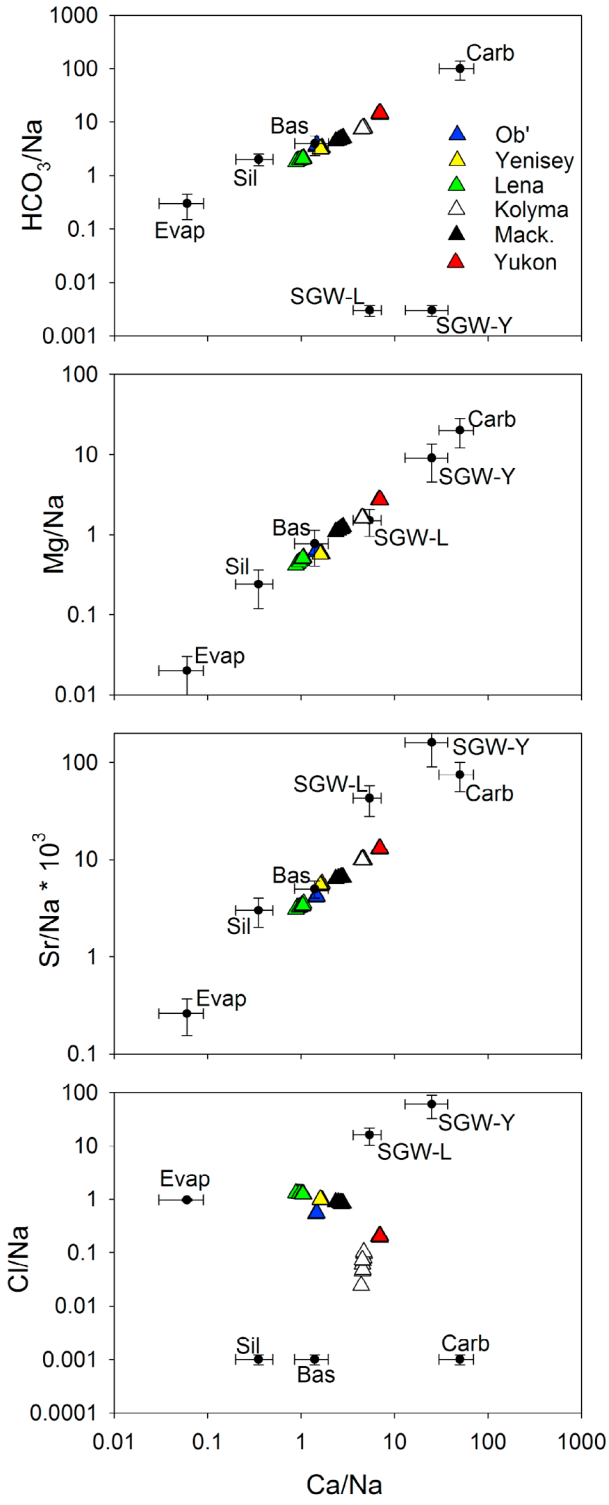

Figure 6. Na-normalized ratios of weathering ions for the six largest Arctic Rivers. Weathering end-members, and standard deviations for their estimate, are shown for carbonates (carb), basalts (bas), silicates (sil), evaporates (evap), and saline groundwater (SGW) from the Lena and Yenisey basins. Note that not all end-members were used for all model runs. Model results are presented in Table 4.

for several Arctic locations [*Walvoord and Striegl*, 2007; *St. Jacques and Sauchyn*, 2009; *Keller et al.*, 2010], indicate an ongoing transition in the effect of permafrost on DIC flux from Arctic rivers. Across the ten sea basins that we model, decreasing the extent of continuous permafrost by 10% results in a 3–10% increase in DIC flux. In addition, the positive relationship between runoff and DIC flux (Figure 3 and Table 2), suggests that the effect of changing permafrost extent on DIC flux could be amplified by the continued increase in runoff that is expected throughout the pan-arctic basin [*Peterson et al.*, 2002; *Déry et al.*, 2009; *Rawlins et al.*, 2010]. However, given the strong seasonal variation in DIC concentration (Figure 2), the magnitude of this effect will depend on when, seasonally, increases in discharge occur.

3.5. The Source of DIC to Major Arctic Rivers

[37] Constituent ratios from the six largest Arctic rivers showed a clear pattern of variation that was much stronger between rivers than it was within rivers between years (Figure 6). For all constituents except Cl^-, the Yukon, Mackenzie, and Kolyma Rivers lay much closer to the carbonate end-member than the Ob', Yenisey, and Lena. In contrast, Cl^-:Na^+ ratios were high on all rivers except the Yukon and Kolyma, indicating a notable contribution of saline waters to the high Cl^-:Na^+ rivers' solute flux. For the Yenisey and Lena Rivers, Cl^-:Na^+ was typically greater than 1, indicating the presence of saline groundwater in the constituent load [see also *Gaillardet et al.*, 1999]. Because saline waters add high concentrations of both Cl^- and Na^+, their effect is to depress the constituent: Na ratio for non-Cl constituents, and we include both saline evaporite and saline groundwater as end-members in our models to correct for this effect.

[38] Between 72 and 81% of the total bicarbonate load from the six PARTNERS rivers was modeled to originate from the weathering of carbonate rocks, with the incorporation of a basaltic, rather than felsic, end-member always decreasing the carbonate contribution (Table 4). Results using the minimum and maximum correction for rainwater were almost identical to each other (average 1.5% difference in carbonate contribution), and thus model outcomes using the mean rainwater correction are presented (Table 4). On average, these large, Arctic rivers are notably above the global mean of roughly two-thirds of riverine bicarbonate originating from carbonate rock weathering (*Meybeck* [1987]; given the assumption that CO_2 consumption by

Table 4. The Percent Contribution of Silicate and Carbonate Weathering to Bicarbonate Flux in the Six Largest Arctic Rivers[a]

River	Percent Contribution	
	Silicates	Carbonates
Ob'	22.1 (0.7)	77.9 (0.8)
Yenisey	38.7 (4.0)–54.7 (6.7)	45.3 (6.3)–61.3 (3.4)
Lena	18.5 (4.2)–32.1 (6.2)	67.9 (6.2)–81.5 (5.9)
Kolyma	21.6 (0.6)–42.2 (1.2)	57.8 (1.2)–78.4 (0.6)
Yukon	9.2 (0.3)–18.8 (0.6)	81.2 (0.6)–90.8 (0.3)
Mackenzie	3.2 (0.5)	96.8 (0.5)
TOTAL	19.4–27.9	72.1–80.6

[a]Standard deviations are given in brackets. Where a range of estimates exists, the lower silicate estimate (higher carbonate estimate) was calculated using the felsic end-member, and the higher silicate estimate (lower carbonate estimate) was calculated using the basaltic end-member.

carbonate weathering is balanced by carbonate rock dissolution; *Aminotte Suchet and Probst* [1995]; *Gaillardet et al.* [1999]). Within rivers, the Mackenzie and Yukon are notably dominated by carbonate weathering, while the Yenisey and Kolyma, which possess a large proportion of basalts, are much more notably influenced by silicate weathering (Table 4). Although carbonates are sparse in the Ob' River basin (Table 2), basalts are almost entirely absent, and the relatively low-yield bicarbonate flux is still largely dominated by carbonates (Table 4). This result may reflect the presence of trace calcite in the rocks of this catchment, in classifications such as 'complex lithology' or others [*Hartmann et al.*, 2009; *Moosdorf et al.*, 2011]. In the Lena River, carbonates are relatively abundant compared to basalts (Table 2), suggesting that the felsic end-member model with its high contribution from carbonates is a more likely scenario (Table 4).

[39] For the Mackenzie and Yukon rivers, our finding of a high proportion of (HCO_3^- + CO_3^{2-}) flux derived from carbonate rock weathering is very similar to the findings of other authors [*Gaillardet et al.*, 1999; *Millot et al.*, 2003]. For the Ob', Yenisey, and Lena rivers, however, we find a noticeably lower contribution of carbonate rock weathering than in previous work [*Gaillardet et al.*, 1999], despite our use of similar values for the carbonate and felsic silicate end-members (detailed in the auxiliary material). In part, this is likely caused by the lower range estimate that results from the inclusion of a basaltic end-member. However, our non-Cl^- constituent ratios for these central Siberian rivers are also as much as 2.3-fold lower than those used by *Gaillardet et al.* [1999], as a result of our use of concentration measurements from across the full seasonal cycle to derive yearly constituent flux estimates, rather than single point measurements of concentration.

[40] Estimating carbonate and silicate rock weathering in these catchments allows us to evaluate weathering-mediated CO_2 consumption within the PARTNERS watersheds. Recently, the oxidative weathering of pyrite (OWP) has been shown to significantly contribute to weathering in the Mackenzie watershed and elsewhere, suggesting that this weathering mechanism may also be underestimated globally [*Calmels et al.*, 2007; *Raymond and Oh*, 2009]. The OWP results in the formation of sulfuric acid which then instigates rock dissolution without the consumption of CO_2 (equations (5) and (6), for carbonate rocks):

$$FeS_2 + \frac{15}{4}O_2 + \frac{7}{2}H_2O \rightarrow Fe(OH)_3 + 2H_2SO_4 \quad (5)$$

$$2CaCO_3 + H_2SO_4 \rightarrow 2Ca^{2+} + 2HCO_3^- + SO_4^{2-} \quad (6)$$

In the Mackenzie basin, OWP is estimated to account for 82% of dissolved SO_4^{2-} flux, and the heavy load of SO_4^{2-} in this river (Table 1), and high proportion of weathering by carbonate rock (Table 4) [*Millot et al.*, 2003], considerably lessens estimates of weathering-mediated CO_2 consumption [*Calmels et al.*, 2007]. To calculate a minimum estimate of weathering-mediated CO_2 consumption, we allow 82% of the Mackenzie SO_4^{2-} flux, and all SO_4^{2-} flux from the remaining PARTNERS rivers, to participate in reaction (6). We then assume that half of the remaining carbonate rock-derived HCO_3^-, and all of the silicate rock-derived HCO_3^-, comes from CO_2 fixation (equations (1) and (2)). This results in a CO_2 consumption estimate of 11.9–13.1 Tg C yr^{-1}. If SO_4^{2-} is assumed to not be derived from OWP on all rivers except the Mackenzie, then a CO_2 consumption estimate of 14.9–16.1 Tg C yr^{-1} results.

[41] These estimates range from 44 to 59% of the total (HCO_3^- + CO_3^{2-}) flux from these rivers (Table 1), considerably less than the global average of two-thirds of DIC flux resulting from CO_2 fixation [e.g., *Meybeck*, 1987]. Although the carbonate-rich nature of these watersheds leads to river water that is relatively concentrated in DIC, it also increases the proportion of DIC that is derived directly from the continental crust. Within individual watersheds, the effect of OWP and the relative proportion of DIC derived from carbonate weathering had a significant impact on the potential aerial yield of weathering-mediated CO_2 fixation. While CO_2 fixation yields were low in the Kolyma, Mackenzie, and Ob' watersheds (range of 0.4–1.0 g C m^{-2} yr^{-1}), they were much higher in the Yenisey and Yukon watersheds (range of 1.6–2.9 g C m^{-2} yr^{-1}). As discussed previously [*Calmels et al.*, 2007], the Mackenzie River basin stands out as having a particularly low proportion of its bicarbonate flux derived from CO_2 fixation.

3.6. Seasonal Variation in Riverine $CaCO_3$ Flux and Its Effect on Coastal Aragonite Saturation

[42] Mean monthly concentrations of riverine carbonate alkalinity and Ca^{2+} show a clear, seasonal trend that varies synchronously across all rivers (Figure 7). For both constituents, concentrations were lowest during and immediately after the spring freshet in June, and highest under ice (Figure 7). Although the pattern for DIC is similar, the wintertime increase in DIC is much more pronounced than for alkalinity (Figure 7), as a result of organic matter mineralization and CO_2 accumulation with a resultant pH shift under ice. This seasonal augmentation of DIC concentration relative to alkalinity leads in-river wintertime concentrations of CO_3^{2-} to fall to near zero levels in all rivers, despite high under-ice carbonate alkalinity concentrations (data not shown).

[43] Previous authors have calculated that riverine-influenced nearshore areas should be particularly susceptible to the effects of ocean acidification, because river water typically has lower carbonate and bicarbonate concentrations than the ocean, and thus the ongoing depression in Ω_{arag} caused by oceanic absorption of CO_2 is compounded on river-influenced shelves [*Salisbury et al.*, 2008; *Aufdenkampe et al.*, 2011]. In the Arctic, which is particularly susceptible to the effects of ocean acidification [*Steinacher et al.*, 2009], plumes of water with low Ω_{arag} have been noted at the mouths of both the Mackenzie and Yukon Rivers [*Chierici and Fransson*, 2009; *Mathis et al.*, 2011], while waters at depth in the East Siberian Sea have also been shown to have notably low Ω_{arag} [*Anderson et al.*, 2011]. We constructed theoretical mixing curves for Ω_{arag} across surface water estuarine gradients, to explore seasonal and geographic patterns in riverine influence on Ω_{arag} in the Arctic Ocean. Curves were constructed for spring and late summer at salinities between 10 and 32. To specifically explore the effect of river water on coastal Ω_{arag}, we ignore the potential effect of sea ice melt in our calculations (but see Conclusions). Across all rivers, and in both seasons, the flux of river water caused Ω_{arag} to be under-saturated

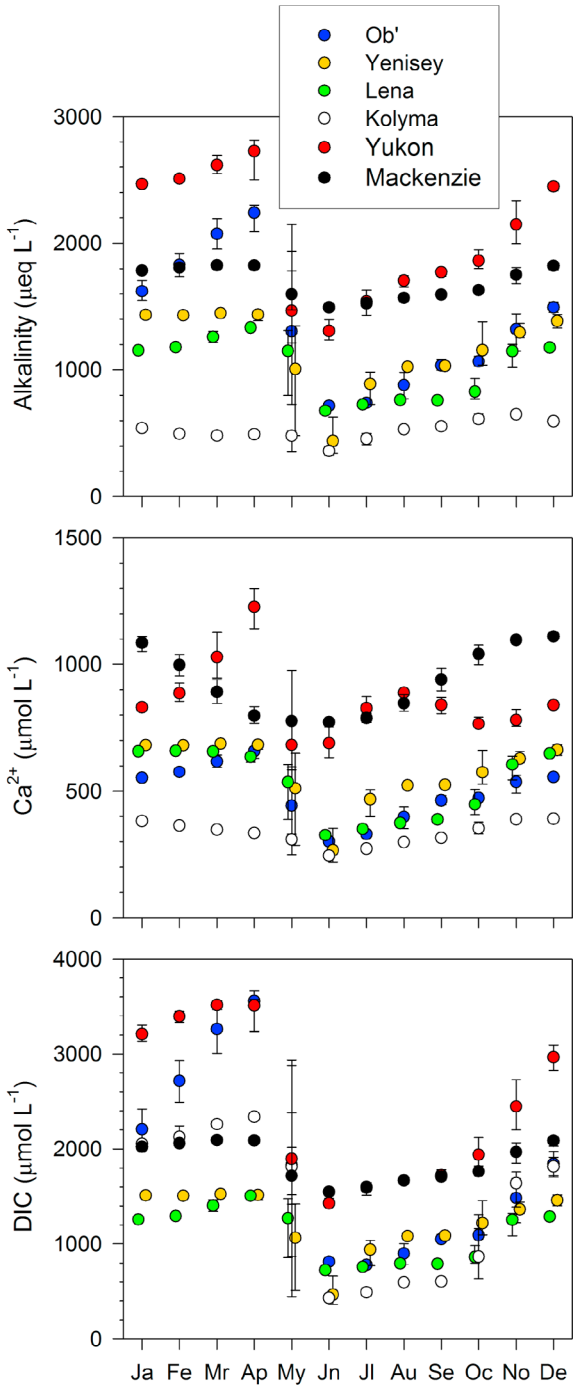

Figure 7. Monthly mean riverine concentrations of alkalinity, Ca^{2+} and DIC from major Arctic rivers, with error bars indicating 5th and 95th percentiles of LOADEST daily concentration estimates.

across broad estuarine gradients (Figure 8). However, there was notable seasonal and regional variation in the reach of under-saturation. Within rivers, the Ω_{arag} end-member was always more dilute in the spring than in the late summer (Figure 8). Between rivers, Ω_{arag} was highest for North America, and lowest for the Kolyma River. Because of the uncertainty of a wintertime oceanic end-member for alkalinity and DIC, we do not display an estuarine mixing curve for wintertime conditions in Figure 8. However, even assuming a wintertime oceanic Ω_{arag} that is higher than our spring/summer end-member (under-ice oceanic DIC = 2230 μmol L^{-1} [*Bates*, 2006] and pCO_2 = 225 μatm [*Bates*, 2006; *Cai et al.*, 2010]) nearshore Ω_{arag} is considerably depressed in the winter compared to the spring and summer: at a salinity of 10, wintertime Ω_{arag} is 0.0 offshore of the Kolyma River, and 0.1 for North American rivers and central Siberia. In all cases, the theoretical wintertime zone of $\Omega_{arag} < 1$ extends farther into the estuarine plume than for the spring or summer. Constructing our spring and later-summer mixing curves at 20°C (the maximum temperature observed in these rivers, but certainly high for offshore regions), decreases the region of $\Omega_{arag} < 1$ between 1 and 4 salinity units, but increases divergence between rivers because the effect is smallest on the Kolyma, and largest for North America. Given that maximum river (and ocean) temperatures occur in the late summer, seasonal temperature variations will also accentuate the seasonal patterns in Ω_{arag} that we show in Figure 8.

[44] These findings mirror the observations described by *Mathis et al.* [2011], who found a sizable zone of $\Omega_{arag} < 1$ at the mouth of the Yukon River in the spring, but not in the late summer. One of the fundamental assumptions of these mixing curves, however, is that DIC and alkalinity mix conservatively across the estuarine gradient, despite the fact that the outgassing or biological uptake/production of CO_2 could render this assumption incorrect. For North American rivers, pCO_2 values calculated along these mixing gradients fall below atmospheric equilibrium at salinities between ~10 and 15, which roughly mirrors values found at similar salinities in the Beaufort Sea at times when sea ice melt is minimal [*Mucci et al.*, 2010]. In contrast, pCO_2 along our central Siberian mixing gradient is significantly lower than what has been observed at similar salinities in situ: while our

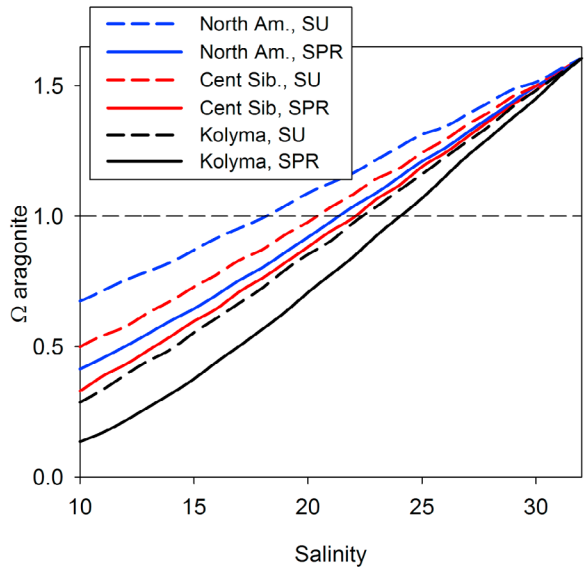

Figure 8. An estimate of seasonal and geographic variation in Ω_{arag} in the coastal Arctic Ocean, based on interpolation between riverine and oceanic end-members. SPR = spring; SU = late summer. The calculated mixing gradient does not include the effects of sea ice melt. Calculation details are given in the text.

mixing curves result in pCO_2 below atmospheric equilibrium at all but the lowest salinities (<13), partial pressures in the Laptev and East Siberian Seas have been observed to be above equilibrium at salinities as high as ~30 [*Anderson et al.*, 2009; *Alling et al.*, 2010].

[45] In part, these anomalies are likely derived from patterns in DIC and DOC export and coastal erosion across the pan-arctic region. While DIC, alkalinity, and coastal Ω_{arag} are highest for North American rivers (Figures 7 and 8) DOC flux and riverine DOC concentrations are substantially higher in Eurasia [*Raymond et al.*, 2007; *Holmes et al.*, 2012], and inputs of particulate organic matter from coastal erosion are also substantial along the Siberian coast [*Vonk et al.*, 2010; *Sánchez-García et al.*, 2011]. In the North American nearshore, therefore, mineralization of terrigenous organic matter to CO_2 should be low, and its effects buffered by higher alkalinities, when compared to the Siberian Arctic. In contrast, the substantial input of terrestrial organic matter from Siberian rivers and coasts decays rapidly in the nearshore region [*Alling et al.*, 2010; *Letscher et al.*, 2011; *Sánchez-García et al.*, 2011], and augments coastal pCO_2 substantially [*Anderson et al.*, 2009]. Thus, terrigenous inorganic and organic C appear to act interactively over Arctic shelves. Variation in DIC:DOC export and coastal erosion across the pan-arctic region should accentuate the regional Ω_{arag} patterns that we show in Figure 8, with coastal Ω_{arag} likely even lower over the Siberian shelves than we calculate by taking only the inorganic component of the C cycle into account. Although sizable areas of $\Omega_{arag} < 1$ have been measured for the Canada Basin and Beaufort, Chukchi, and Bering Seas [e.g., *Bates*, 2006; *Bates et al.*, 2009; *Mathis et al.*, 2011; *Yamamoto-Kawai et al.*, 2011], surface water Ω_{arag} is much less well documented over the Siberian shelf seas (but see *Anderson et al.* [2011]).

4. Conclusions

[46] The seasonally distributed and multiyear data sets that have resulted from the PARTNERS and Arctic-GRO sampling campaigns have enabled us to provide significantly improved flux estimates for DIC and other weathering constituents from the largest Arctic rivers. Compared to other world rivers, these large Arctic rivers are generally DIC-rich, and DIC comprises a strong majority of the dissolved C flux from the pan-arctic watershed. In addition to lithology, DIC flux from these watersheds is controlled by several factors that are known to be changing with climate: runoff [*Rawlins et al.*, 2010], permafrost extent [*Oelke et al.*, 2004], and glacial coverage [*Gardner et al.*, 2011]. Both increasing runoff and decreasing permafrost extent are expected to increase DIC yields [*Raymond and Cole*, 2003; *Walvoord and Striegl*, 2007]. Over the short-term, glacial retreat could also increase DIC flux by increasing the extent of proglacial sediments, which are particularly vulnerable to weathering [*Anderson et al.*, 2000; *Wadham et al.*, 2001]. This, in turn, has clear implications for the magnitude of CO_2 fixation via weathering on land, and the impact of DIC in the coastal Arctic Ocean.

[47] Currently, fluxes of DIC and Ca^{2+} to the coastal Arctic Ocean universally cause river-influenced shelves to be under-saturated in aragonite. Over the full extent of the Arctic Ocean, the effect of sea ice melt on Ω_{arag} is expected to be much greater than the effect of river water, because of the greater volume of meltwater relative to river water, and its extremely dilute nature [*Yamamoto-Kawai et al.*, 2009]. However, we show that the impact of river water will be highest during periods when sea ice melt is minimal, indicating that the delivery of river water to nearshore regions may work to cause sizable regions of under-saturation throughout the annual cycle. In addition, our results suggest that under-saturation should be much greater for riverine-influenced Siberian shelves than for their North American counterparts, indicating a clear need for better in situ measurements of Ω_{arag} in this region. Because the PARTNERS and Arctic-GRO projects provide measurements that are seasonally distributed and collected and analyzed using identical techniques on all rivers, the estimates that we present provide an important baseline for the assessment of future change.

[48] **Acknowledgments.** Funding for this work was provided through NSF-OPP-0229302 and NSF-OPP-0732985. Additional support to SET was provided by an NSERC Postdoctoral Fellowship. Comments from J. Hartmann and one anonymous reviewer greatly improved the content of the manuscript.

References

Alling, V., et al. (2010), Nonconservative behavior of dissolved organic carbon across the Laptev and East Siberian seas, *Global Biogeochem. Cycles*, *24*, GB4033, doi:10.1029/2010GB003834.

Aminotte Suchet, P., and J. L. Probst (1995), A global model for present-day atmospheric soil CO_2 consumption by chemical erosion of continental rocks (GEM-CO_2), *Tellus, Ser. B*, *47*, 273–280, doi:10.1034/j.1600-0889.47.issue1.23.x.

Anderson, L. G., S. Jutterstrom, S. Hjalmarsson, I. Wahlstrom, and I. P. Semiletov (2009), Out-gassing of CO_2 from Siberian Shelf seas by terrestrial organic matter decomposition, *Geophys. Res. Lett.*, *36*, L20601, doi:10.1029/2009GL040046.

Anderson, L. G., G. Bjork, S. Jutterstrom, I. Pipko, N. Shakhova, I. Semiletov, and I. Wahlstrom (2011), East Siberian Sea, an Arctic region of very high biogeochemical activity, *Biogeosciences*, *8*, 1745–1754, doi:10.5194/bg-8-1745-2011.

Anderson, S. P., J. I. Drever, C. D. Frost, and P. Holden (2000), Chemical weathering in the foreland of a retreating glacier, *Geochim. Cosmochim. Acta*, *64*, 1173–1189, doi:10.1016/S0016-7037(99)00358-0.

Aufdenkampe, A. K., E. Mayorga, P. A. Raymond, J. M. Melack, S. C. Doney, S. R. Alin, R. E. Aalto, and K. Yoo (2011), Riverine coupling of biogeochemical cycles between land, oceans, and atmosphere, *Front. Ecol. Environ*, *9*, 53–60, doi:10.1890/100014.

Bates, N. R. (2006), Air-sea CO_2 fluxes and the continental shelf pump of carbon in the Chukchi Sea adjacent to the Arctic Ocean, *J. Geophys. Res.*, *111*, C10013, doi:10.1029/2005JC003083.

Bates, N. R., J. T. Mathis, and L. W. Cooper (2009), Ocean acidification and biologically induced seasonality of carbonate mineral saturation states in the western Arctic Ocean, *J. Geophys. Res.*, *114*, C11007, doi:10.1029/2008JC004862.

Berner, R. A., A. C. Lasaga, and R. M. Garrels (1983), The carbonate-silicate geochemical cycle and its effect on atmospheric carbon dioxide over the past 100 million years, *Am. J. Sci.*, *283*, 641–683, doi:10.2475/ajs.283.7.641.

Booth, G., P. A. Raymond, and N.-H. Oh (2007), LoadRunner, software, Yale Univ., New Haven, Conn. [Available at http://environment.yale.edu/raymond/loadrunner/.]

Brown, J., O. J. Ferrians Jr., J. A. Heginbottom, and E. S. Melnikov (1998), Circum-arctic map of permafrost and ground ice conditions, http://nsidc.org/data/docs/fgdc/ggd318_map_circumarctic/index.html, Natl. Snow and Ice Data Cent., Boulder, Colo.

Cai, W.-J., et al. (2010), Decrease in the CO_2 uptake capacity in an ice-free Arctic Ocean Basin, *Science*, *329*, 556–559, doi:10.1126/science.1189338.

Calmels, D., J. Gaillardet, A. Brenot, and C. France-Lanord (2007), Sustained sulfide oxidation by physical erosion processes in the Mackenzie River basin: Climatic perspectives, *Geology*, *35*, 1003–1006, doi:10.1130/G24132A.1.

Chierici, M., and A. Fransson (2009), Calcium carbonate saturation in the surface water of the Arctic Ocean: Undersaturation in freshwater influenced shelves, *Biogeosciences*, *6*, 2421–2431, doi:10.5194/bg-6-2421-2009.

Cogley, J. G. (2010), A more complete version of the World Glacier Inventory, *Ann. Glaciol.*, *50*, 32–38, doi:10.3189/172756410790595859.

Cooper, L. W., J. W. McClelland, R. M. Holmes, P. A. Raymond, J. J. Gibson, C. K. Guay, and B. J. Peterson (2008), Flow-weighted values of runoff tracers ($\delta^{18}O$, DOC, Ba, alkalinity) from the six largest Arctic rivers, *Geophys. Res. Lett.*, *35*, L18606, doi:10.1029/2008GL035007.

Déry, S. J., M. Stieglitz, E. C. McKenna, and E. F. Wood (2005), Characteristics and trends of river discharge into Hudson, James, and Ungava Bays, 1964–2000, *J. Clim.*, *18*, 2540–2557, doi:10.1175/JCLI3440.1.

Déry, S. J., M. A. Hernandez-Henriquez, J. E. Burford, and E. F. Wood (2009), Observational evidence of an intensifying hydrological cycle in northern Canada, *Geophys. Res. Lett.*, *36*, L13402, doi:10.1029/2009GL038852.

Dessert, C., B. Dupre, J. Gaillardet, L. M. Francois, and C. J. Allegre (2003), Basalt weathering laws and the impact of basalt weathering on the global carbon cycle, *Chem. Geol.*, *202*, 257–273, doi:10.1016/j.chemgeo.2002.10.001.

Doney, S. C., V. J. Fabry, R. A. Feely, and J. A. Kleypas (2009), Ocean acidification: The other CO_2 problem, *Annu. Rev. Mar. Sci.*, *1*, 169–192, doi:10.1146/annurev.marine.010908.163834.

Dornblaser, M. M., and R. G. Striegl (2007), Nutrient (N, P) loads and yields at multiple scales and subbasin types in the Yukon River basin, Alaska, *J. Geophys. Res.*, *112*, G04S57, doi:10.1029/2006JG000366.

Dürr, H. H., M. Meybeck, and S. H. Durr (2005), Lithologic composition of the Earth's continental surfaces derived from a new digital map emphasizing riverine material transfer, *Global Biogeochem. Cycles*, *19*, GB4S10, doi:10.1029/2005GB002515.

Emmerton, C. A., L. F. W. Lesack, and W. F. Vincent (2008), Mackenzie River nutrient delivery to the Arctic Ocean and effects of the Mackenzie Delta during open water conditions, *Global Biogeochem. Cycles*, *22*, GB1024, doi:10.1029/2006GB002856.

Environment Canada (1978), *Water Quality Data: Manitoba 1961–1976*, Inland Waters Dir., Ottawa.

Feely, R. A., C. L. Sabine, K. Lee, W. Berelson, J. Kleypas, V. J. Fabry, and F. J. Millero (2004), Impact of anthropogenic CO_2 on the $CaCO_3$ system in the oceans, *Science*, *305*, 362–366, doi:10.1126/science.1097329.

Fekete, B. M., C. J. Vörösmarty, and W. Grabs (2002), High-resolution fields of global runoff combining observed river discharge and simulated water balances, *Global Biogeochem. Cycles*, *16*(3), 1042, doi:10.1029/1999GB001254.

Frey, K. E., and J. W. McClelland (2009), Impacts of permafrost degradation on Arctic River biogeochemistry, *Hydrol. Processes*, *23*, 169–182, doi:10.1002/hyp.7196.

Frey, K. E., D. I. Siegel, and L. C. Smith (2007), Geochemistry of west Siberian streams and their potential response to permafrost degradation, *Water Resour. Res.*, *43*, W03406, doi:10.1029/2006WR004902.

Gaillardet, J., B. Dupre, P. Louvat, and C. J. Allegre (1999), Global silicate weathering and CO_2 consumption rates deduced from the chemistry of large rivers, *Chem. Geol.*, *159*, 3–30, doi:10.1016/S0009-2541(99)00031-5.

Gardner, A. S., G. Moholdt, B. Wouters, G. J. Wolken, D. O. Burgess, M. J. Sharp, J. G. Cogley, C. Braun, and C. Labine (2011), Sharply increased mass loss from glaciers and ice caps in the Canadian Arctic Archipelago, *Nature*, *473*, 357–360, doi:10.1038/nature10089.

Gordeev, V. V., J. M. Martin, I. S. Sidorov, and M. V. Sidorova (1996), A reassessment of the Eurasian river input of water, sediment, major elements, and nutrients to the Arctic Ocean, *Am. J. Sci.*, *296*, 664–691, doi:10.2475/ajs.296.6.664.

Harsch, M. A., P. E. Hulme, M. S. McGlone, and R. P. Duncan (2009), Are treelines advancing? A global meta-analysis of treeline response to climate warming, *Ecol. Lett.*, *12*, 1040–1049, doi:10.1111/j.1461-0248.2009.01355.x.

Hartmann, J., N. Jansen, H. H. Durr, S. Kempe, and P. Kohler (2009), Global CO_2-consumption by chemical weathering: What is the contribution of highly active weathering regions?, *Global Planet. Change*, *69*, 185–194, doi:10.1016/j.gloplacha.2009.07.007.

Hodgkins, R., M. Tranter, and J. A. Dowdeswell (1997), Solute provenance, transport and denudation in a High Arctic glacierized catchment, *Hydrol. Processes*, *11*, 1813–1832, doi:10.1002/(SICI)1099-1085(199711)11:14<1813::AID-HYP498>3.0.CO;2-C.

Hodson, A., M. Tranter, and G. Vatne (2000), Contemporary rates of chemical denudation and atmospheric CO_2 sequestration in glacier basins: An Arctic perspective, *Earth Surf. Processes Landforms*, *25*, 1447–1471, doi:10.1002/1096-9837(200012)25:13<1447::AID-ESP156>3.0.CO;2-9.

Holmes, R. M., B. J. Peterson, V. V. Gordeev, A. V. Zhulidov, M. Meybeck, R. B. Lammers, and C. J. Vorosmarty (2000), Flux of nutrients from Russian rivers to the Arctic Ocean: Can we establish a baseline against which to judge future changes?, *Water Resour. Res.*, *36*, 2309–2320, doi:10.1029/2000WR900099.

Holmes, R. M., B. J. Peterson, A. V. Zhulidov, V. V. Gordeev, P. N. Makkaveev, P. A. Stunzhas, L. S. Kosmenko, G. H. Kohler, and A. I. Shiklomanov (2001), Nutrient chemistry of the Ob' and Yenisey Rivers, Siberia: Results from June 2000 expedition and evaluation of long-term data sets, *Mar. Chem.*, *75*, 219–227, doi:10.1016/S0304-4203(01)00038-X.

Holmes, R. M., et al. (2012), Seasonal and annual fluxes of nutrients and organic matter from large rivers to the Arctic Ocean and surrounding seas, *Estuaries Coasts*, *35*(2), 369–382.

Kaser, G., M. Großhauser, and B. Marzeion (2010), Contribution potential of glaciers to water availability in different climate regimes, *Proc. Natl. Acad. Sci. U. S. A.*, *107*, 20,223–20,227, doi:10.1073/pnas.1008162107.

Keller, K., J. D. Blum, and G. W. Kling (2010), Stream geochemistry as an indicator of increasing permafrost thaw depth in an arctic watershed, *Chem. Geol.*, *273*, 76–81, doi:10.1016/j.chemgeo.2010.02.013.

Kump, L. R., and R. B. Alley (1994), Global chemical weathering on glacial time scales, in *Material Fluxes on the Surface of the Earth*, edited by N. R. C. Board on Earth Sciences and Resources, pp. 46–60, Natl. Acad. Press, Washington, D. C.

Lammers, R. B., A. I. Shiklomanov, C. J. Vorosmarty, B. M. Fekete, and B. J. Peterson (2001), Assessment of contemporary Arctic river runoff based on observational discharge records, *J. Geophys. Res.*, *106*, 3321–3334, doi:10.1029/2000JD900444.

Letscher, R. T., D. A. Hansell, and D. Kadko (2011), Rapid removal of terrigenous dissolved organic carbon over the Eurasian shelves of the Arctic Ocean, *Mar. Chem.*, *123*, 78–87, doi:10.1016/j.marchem.2010.10.002.

Lewis, E., and D. Wallace (1998), CO2SYS: Program developed for CO_2 system calculations, report, Carbon Dioxide Inf. Anal. Cent., Oak Ridge, Tenn., doi:10.2172/639712.

Louvat, P., S. R. Gislason, and C. J. Allegre (2008), Chemical and mechanical erosion rates in Iceland as deduced from river dissolved and solid material, *Am. J. Sci.*, *308*, 679–726, doi:10.2475/05.2008.02.

Mackenzie, F. T., and R. M. Garrels (1966), Chemical mass balance between rivers and oceans, *Am. J. Sci.*, *264*, 507–525, doi:10.2475/ajs.264.7.507.

Mathis, J. T., J. N. Cross, and N. R. Bates (2011), Coupling primary production and terrestrial runoff to ocean acidification and carbonate mineral suppression in the eastern Bering Sea, *J. Geophys. Res.*, *116*, C02030, doi:10.1029/2010JC006453.

McClelland, J. W., S. J. Dery, B. J. Peterson, R. M. Holmes, and E. F. Wood (2006), A pan-arctic evaluation of changes in river discharge during the latter half of the 20th century, *Geophys. Res. Lett.*, *33*, L06715, doi:10.1029/2006GL025753.

McClelland, J. W., M. Stieglitz, F. Pan, R. M. Holmes, and B. J. Peterson (2007), Recent changes in nitrate and dissolved organic carbon export from the upper Kuparuk River, North Slope, Alaska, *J. Geophys. Res.*, *112*, G04S60, doi:10.1029/2006JG000371.

McClelland, J. W., et al. (2008), Development of a pan-Arctic database for river chemistry, *Eos Trans. AGU*, *89*(24), 217, doi:10.1029/2008EO240001.

McClelland, J. W., R. M. Holmes, K. H. Dunton, and R. W. Macdonald (2012), The Arctic Ocean estuary, *Estuaries Coasts*, *35*(2), 353–368.

McGuire, A. D., L. G. Anderson, T. R. Christensen, S. Dallimore, L. D. Guo, D. J. Hayes, M. Heimann, T. D. Lorenson, R. W. Macdonald, and N. Roulet (2009), Sensitivity of the carbon cycle in the Arctic to climate change, *Ecol. Monogr.*, *79*, 523–555, doi:10.1890/08-2025.1.

McGuire, A. D., et al. (2010), An analysis of the carbon balance of the Arctic Basin from 1997 to 2006, *Tellus Ser. B*, *62*, 455–474, doi:10.1111/j.1600-0889.2010.00497.x.

Meybeck, M. (1987), Global chemical weathering of surficial rocks estimated from river dissolved loads, *Am. J. Sci.*, *287*, 401–428, doi:10.2475/ajs.287.5.401.

Meybeck, M., and A. Ragu (1995), River discharges to the oceans: An assessment of suspended solids, major ions and nutrients, report, U. N. Envrion. Programme, Geneva, Switzerland.

Millero, F. J. (1979), Thermodynamics of the carbonate system in seawater, *Geochim. Cosmochim. Acta*, *43*, 1651–1661, doi:10.1016/0016-7037(79)90184-4.

Millero, F. J. (2010), Carbonate constants for estuarine waters, *Mar. Freshwater Res.*, *61*, 139–142, doi:10.1071/MF09254.

Millot, R., J. Gaillardet, B. Dupre, and C. J. Allegre (2003), Northern latitude chemical weathering rates: Clues from the Mackenzie River Basin, Canada, *Geochim. Cosmochim. Acta*, *67*, 1305–1329, doi:10.1016/S0016-7037(02)01207-3.

Moore, J. W., and B. X. Semmens (2008), Incorporating uncertainty and prior information into stable isotope mixing models, *Ecol. Lett.*, *11*, 470–480, doi:10.1111/j.1461-0248.2008.01163.x.

Moosdorf, N., J. Hartmann, R. Lauerwald, B. Hagedorn, and S. Kempe (2011), Atmospheric CO_2 consumption by chemical weathering in North America, *Geochim. Cosmochim. Acta*, *75*, 7829–7854, doi:10.1016/j.gca.2011.10.007.

Mucci, A. (1983), The solubility of calcite and aragonite in seawater at various salinities, temperatures, and one atmosphere total pressure, *Am. J. Sci.*, *283*, 780–799, doi:10.2475/ajs.283.7.780.

Mucci, A., B. Lansard, L. A. Miller, and T. N. Papakyriakou (2010), CO_2 fluxes across the air-sea interface in the southeastern Beaufort Sea: Ice-free period, *J. Geophys. Res.*, *115*, C04003, doi:10.1029/2009JC005330.

Oelke, C., T. Zhang, and M. C. Serreze (2004), Modeling evidence for recent warming of the Arctic soil thermal regime, *Geophys. Res. Lett.*, *31*, L07208, doi:10.1029/2003GL019300.

Oliver, B. G., E. M. Thurman, and R. L. Malcolm (1983), The contribution of humic substances to the acidity of colored natural waters, *Geochim. Cosmochim. Acta*, *47*, 2031–2035, doi:10.1016/0016-7037(83)90218-1.

Perrin, A. S., A. Probst, and J. L. Probst (2008), Impact of nitrogenous fertilizers on carbonate dissolution in small agricultural catchments: Implications for weathering CO_2 uptake at regional and global scales, *Geochim. Cosmochim. Acta*, *72*, 3105–3123, doi:10.1016/j.gca.2008.04.011.

Peterson, B. J., R. M. Holmes, J. W. McClelland, C. J. Vorosmarty, R. B. Lammers, A. I. Shiklomanov, I. A. Shiklomanov, and S. Rahmstorf (2002), Increasing river discharge to the Arctic Ocean, *Science*, *298*, 2171–2173, doi:10.1126/science.1077445.

Rawlins, M. A., et al. (2010), Analysis of the Arctic system for freshwater cycle intensification: Observations and expectations, *J. Clim.*, *23*, 5715–5737, doi:10.1175/2010JCLI3421.1.

Raymond, P. A., and J. J. Cole (2003), Increase in the export of alkalinity from North America's largest river, *Science*, *301*, 88–91, doi:10.1126/science.1083788.

Raymond, P. A., and N.-H. Oh (2009), Long term changes of chemical weathering products in rivers heavily impacted from acid mine drainage: Insights on the impact of coal mining on regional and global carbon and sulfur budgets, *Earth Planet. Sci. Lett.*, *284*, 50–56, doi:10.1016/j.epsl.2009.04.006.

Raymond, P. A., J. W. McClelland, R. M. Holmes, A. V. Zhulidov, K. Mull, B. J. Peterson, R. G. Striegl, G. R. Aiken, and T. Y. Gurtovaya (2007), Flux and age of dissolved organic carbon exported to the Arctic Ocean: A carbon isotopic study of the five largest arctic rivers, *Global Biogeochem. Cycles*, *21*, GB4011, doi:10.1029/2007GB002934.

Riley, J. P., and M. Tongudai (1967), The major cation/chlorinity ratios in sea water, *Chem. Geol.*, *2*, 263–269, doi:10.1016/0009-2541(67)90026-5.

Runkel, R. L., C. G. Crawford, and T. A. Cohn (2004), *Load Estimator (LOADEST): A FORTRAN Program for Estimating Constituent Loads in Streams and Rivers, U.S. Geol. Surv. Tech. and Meth.*, book 4, chap. A5, 69 pp., U.S. Geol. Surv., Denver, Colo.

Salisbury, J., M. Green, C. Hunt, and J. Campbell (2008), Coastal acidification by rivers: A threat to shellfish?, *Eos Trans. AGU*, *89*(50), 513, doi:10.1029/2008EO500001.

Sánchez-García, L., V. Alling, S. Pugach, J. Vonk, B. van Dongen, C. Humborg, O. Dudarev, I. Semiletov, and Ö. Gustafsson (2011), Inventories and behavior of particulate organic carbon in the Laptev and East Siberian seas, *Global Biogeochem. Cycles*, *25*, GB2007, doi:10.1029/2010GB003862.

Schlünz, B., and R. R. Schneider (2000), Transport of terrestrial organic carbon to the oceans by rivers: Re-estimating flux- and burial rates, *Int. J. Earth Sci.*, *88*, 599–606, doi:10.1007/s005310050290.

Schuster, P. F. (Ed.) (2003), Water and sediment quality in the Yukon River Basin, Alaksa, during water year 2001, *U.S. Geol. Surv. Open File Rep.*, *03-427*, 120 pp.

Sharp, M., M. Tranter, G. H. Brown, and M. Skidmore (1995), Rates of chemical denudation and CO_2 drawdown in a glacier-covered alpine catchment, *Geology*, *23*, 61–64, doi:10.1130/0091-7613(1995)023<0061:ROCDAC>2.3.CO;2.

Shiller, A. M. (2003), Syringe filtration methods for examining dissolved and colloidal trace element distributions in remote field locations, *Environ. Sci. Technol.*, *37*, 3953–3957, doi:10.1021/es0341182.

Steinacher, M., F. Joos, T. L. Frolicher, G. K. Plattner, and S. C. Doney (2009), Imminent ocean acidification in the Arctic projected with the NCAR global coupled carbon cycle-climate model, *Biogeosciences*, *6*, 515–533, doi:10.5194/bg-6-515-2009.

St. Jacques, J. M., and D. J. Sauchyn (2009), Increasing winter baseflow and mean annual streamflow from possible permafrost thawing in the Northwest Territories, Canada, *Geophys. Res. Lett.*, *36*, L01401, doi:10.1029/2008GL035822.

Striegl, R. G., G. R. Aiken, M. M. Dornblaser, P. A. Raymond, and K. P. Wickland (2005), A decrease in discharge-normalized DOC export by the Yukon River during summer through autumn, *Geophys. Res. Lett.*, *32*, L21413, doi:10.1029/2005GL024413.

Striegl, R. G., M. M. Dornblaser, G. R. Aiken, K. P. Wickland, and P. A. Raymond (2007), Carbon export and cycling by the Yukon, Tanana, and Porcupine rivers, Alaska, 2001–2005, *Water Resour. Res.*, *43*, W02411, doi:10.1029/2006WR005201.

Sundquist, E. T. (1991), Steady- and non-steady-state carbonate-silicate controls on atmospheric CO_2, *Quat. Sci. Rev.*, *10*, 283–296, doi:10.1016/0277-3791(91)90026-Q.

Tranter, M., M. J. Sharp, G. H. Brown, I. C. Willis, B. P. Hubbard, M. K. Nielsen, C. C. Smart, S. Gordon, M. Tulley, and H. R. Lamb (1997), Variability in the chemical composition of in situ subglacial meltwaters, *Hydrol. Processes*, *11*, 59–77, doi:10.1002/(SICI)1099-1085(199701)11:1<59::AID-HYP403>3.0.CO;2-S.

Vetrov, A. A., and E. R. Romankevich (2004), *Carbon Cycling in the Russian Arctic Seas*, Springer, Berlin.

Vonk, J. E., L. Sanchez-Garcia, I. Semiletov, O. Dudarev, T. Eglinton, A. Andersson, and O. Gustafsson (2010), Molecular and radiocarbon constraints on sources and degradation of terrestrial organic carbon along the Kolyma paleoriver transect, East Siberian Sea, *Biogeosciences*, *7*, 3153–3166, doi:10.5194/bg-7-3153-2010.

Wadham, J. L., R. J. Cooper, M. Tranter, and R. Hodgkins (2001), Enhancement of glacial solute fluxes in the proglacial zone of a polythermal glacier, *J. Glaciol.*, *47*, 378–386, doi:10.3189/172756501781832188.

Wadham, J. L., M. Tranter, M. Skidmore, A. J. Hodson, J. Priscu, W. B. Lyons, M. Sharp, P. Wynn, and M. Jackson (2010), Biogeochemical weathering under ice: Size matters, *Global Biogeochem. Cycles*, *24*, GB3025, doi:10.1029/2009GB003688.

Walvoord, M. A., and R. G. Striegl (2007), Increased groundwater to stream discharge from permafrost thawing in the Yukon River basin: Potential impacts on lateral export of carbon and nitrogen, *Geophys. Res. Lett.*, *34*, L12402, doi:10.1029/2007GL030216.

World Glacier Monitoring Service (1989), *World Glacier Inventory - Status 1988*, edited by W. Haeberli et al., World Glacier Monitor. Serv., Zurich, Switzerland.

Yamamoto-Kawai, M., F. A. McLaughlin, E. C. Carmack, S. Nishino, and K. Shimada (2009), Aragonite undersaturation in the Arctic Ocean: Effects of ocean acidification and sea ice melt, *Science*, *326*, 1098–1100, doi:10.1126/science.1174190.

Yamamoto-Kawai, M., F. A. McLaughlin, and E. C. Carmack (2011), Effects of ocean acidification, warming and melting of sea ice on aragonite saturation of the Canada Basin surface water, *Geophys. Res. Lett.*, *38*, L03601, doi:10.1029/2010GL045501.

Zakharova, E. A., O. S. Pokrovsky, B. Dupre, J. Gaillardet, and L. E. Efimova (2007), Chemical weathering of silicate rocks in Karelia region and Kola peninsula, NW Russia: Assessing the effect of rock composition, wetlands and vegetation, *Chem. Geol.*, *242*, 255–277, doi:10.1016/j.chemgeo.2007.03.018.